TURUN YLIOPISTO

Implementation of a monitoring add-on for oxygen-15 labelled water administration system in PET/CT

Masters Degree Programme in Biomedical Imaging

Masters Thesis

Jussi Tirkkonen

1.4.2025

Turku

Masters Thesis

Degree programme: Masters Degree Programme in Biomedical Imaging, Faculty of Medicine, Institute of Biomedicine

Author: Jussi Tirkkonen

Title: Implementation of a monitoring add-on for oxygen-15 labelled water administration system in PET/CT

Supervisors:

1. Dr. Reetta Siekkinen - Medical Physicist, Turku PET Centre, University of Turku
2. Dr. Jarmo Teuho - Adjunct Professor (title of Docent), Turku PET Centre, University of Turku
3. Prof. Riku Klén - Associate Professor (Imaging instrumentation and detection technologies) Turku PET Centre, University of Turku

Pages: 55 pp., 1 Appendix

Date: 1.4.2025

Keywords: PET imaging, Radiotracer, Oxygen-15, Medical Instrumentation

Abstract

Positron emission tomography (PET) is a highly advanced non-invasive imaging technology that allows the acquisition of detailed internal images. PET imaging is applied in multiple fields such as clinical oncology and cardiac perfusion studies. PET employs radioactively labelled components known as radiotracers, to act as biological labels in imaging procedures. Radiotracers are administered to the patient prior to image acquisition. Due to the nuclear instability of these radiotracers, they are considered as radiotoxic substances, and the administration process needs to be monitored rigorously to ensure the safety of patients and operation staff. One of the most significant radiotracers in cardiovascular imaging is oxygen-15 labelled water [^{15}O-H_2O] also known as radiowater. It is used in clinical and research applications throughout the world. The gold standard for radiowater production instruments is the Hidex Radiowater Generator (RWG). The current system, however, has limitations that Turku PET Centre together with the manufacturer Hidex Oy is aiming to overcome with the implementation of a monitoring unit that can be installed parallel to an existing RWG setup. This implementation is a part of a larger project titled WASP, (Radio)Water Administration Standardisation Project.

In this research project, the said add-on was installed to three existing RWG systems and standard procedure runs were performed according to Turku PET Centre protocol. A total of 29 measurements were completed and recorded, from which the stability and repeatability of the add-on was evaluated. Evaluation was carried out by comparing both individual and total data regarding the pressure and component flow similarity and the bolus curve characteristics. In this project the implementation was successful, and the system was found to be stable regarding all monitored factors. Possible instability within the systems was justified as instrumentation variance, unrelated to the add-on. The add-on was deemed interchangeable within different RWG systems.

Table of contents

List of abbreviations

Abbreviation	Meaning
AUC	Area Under the Curve
CPS	Counts Per Second
CT	Computed Tomography
EoL	End of Line
FDG	[^{18}F]-Fluorodeoxyglucose
FWHM	Full Width at Half Maximum
MAF	Mass Air Flow
MBF	Myocardial Blood Flow
MRI	Magnetic Resonance Imaging
PET	Positron Emission Tomography
PLC	Programmable Logic Controller
PMT	Photomultiplier Tube
[^{15}O-H_2O]	Radiowater
RWG	Radiowater Generator
SiPM	Silicon Photomultiplier
UI	User Interface

1 Overview

1.1 Introduction

In all medical procedures that benefit from the use of ionising radiation the main aspects are justification and minimisation of use. Justification meaning the gained result or information outweighing the potential harm that is caused to the patient, and minimisation meaning the exposure to lowest possible dose that meaningful results can be achieved with. In order to optimise the procedures regarding the minimisation principle, it is vital to know all factors affecting the patient exposure. [1]

Positron Emission Tomography (PET) is a non-invasive imaging method that utilises radioactive substances known as radiotracers. Radiotracers contain a positron emitting component, which is an ionising radiation source. These radiotracers are most commonly administered to the patient intravenously. Infusion devices are a known source of errors in intravenous administration, and in order to gain a complete understanding of the administration procedure all physical factors affecting the infusion need to be known. [2][3]

Together with Turku PET Centre Hidex Oy has developed a prototype of a monitoring add-on for Oxygen-15 labelled water [^{15}O-H_2O] (also known as radiowater) administration systems. This add-on can be installed parallel to a radiowater generator (RWG) that is a clinically used radiowater production and administration unit. This add-on is developed to gain a better understanding of the physical factors of radiowater production and the administration procedure. This add-on includes components that provide information regarding the physical characteristics, such as component pressure and flow rate within the system and monitor the movements of radioactive material inside the system in different phases of the procedure. This master's thesis is carried out as an implementation of said add-on, and evaluation of its functionality as a pre-clinical research device.

1.2 Thesis structure

This thesis consists of seven chapters excluding the acknowledgements, references and appendices chapters. Out of these seven chapters six of them contain sub-chapters as the information presented in these chapters is reasonable to parse into separate sections. The thesis begins by familiarising the reader with the motivation and previous studies conducted with this matter and then proceeds to present the aim of the study and research questions. The following background section contains relevant technical information regarding the systems and processes that are involved in the project but not directly the topic of research, such as the working principle of a PET scanner or the state of radiowater as a radiotracer in PET. The Materials and methods section presents the directly involved components of this project, including the composition and working principle of the monitoring add-on and information about how these measurements were conducted. The Materials and methods section also includes an explanation of why each of the measurements was conducted. Results chapter presents all the results acquired. Each sub-chapter in results also points out the potential abnormalities and causes (if known) in the data. The acquired results are evaluated in the discussion chapter which is constructed on the basis of the aim of the study and research questions.

1.3 Motivation

This thesis is a part of a larger project carried out within the Turku PET Centre titled WASP (Radio) Water Administration Standardisation Project. Dr. Siekkinen and Dr. Teuho are the responsible authorities for this project. The aim of the WASP project is to standardise and unify the radiowater administration processes nationally. In the WASP project there are multiple radiowater users involved throughout Finnish imaging facilities, such as Kuopio University Hospital and Helsinki University Hospital. All parties in the WASP project are conducting research with radiowater, but Turku PET Centre is the first one to have access to this monitoring add-on which upon successful implementation could provide more relevant data for all parties in their radiowater standardisation procedures.

Radiowater is in most cases administered intravenously to the patient. Intravenous administration has multiple advantages, including precise dosing rate as closing the infusion port stops the drug administration process. When substances (in this case radiotracers) are administered intravenously there is, however, a possibility to cause interference with the administration process itself. This interference could be happening due to movement artefacts, instrumentation variance or a source of back pressure to the system. The introduced back pressure (or the lack of it) could alter the

administration process speed, which would result in falsely calibrated volume of radiotracer to be injected into the patient. As of now, there is no system available to monitor the effects of backpressure in radiowater administration, that would encompass all the physical factors in this process. This previously described monitoring add-on could act as such a system, and if deemed suitable for preclinical research it could play a significant part in, for example, Myocardial Blood Flow (MBF) studies. [4][6]

1.4 Previous studies

The stability and measurement uncertainty of RWG systems has been previously evaluated in a master's thesis written by Milja Siikonen (MSc). This thesis was published in 2024 and is titled *"Measurement uncertainty of the bolus curves produced by a radiowater generator"*. In this thesis the bolus curves produced by different RWG systems were evaluated in repeated measurements. The data recorded in this thesis was extracted from the RWG system user software. In this thesis the bolus curves produced by different RWG systems were deemed to be repeatable regarding the curve peak and width, and the measurement uncertainty was found to be below the limit declared by the system provider. The bolus curves were evaluated regarding the curve peak, Full Width at Half Maximum (FWHM) and Area Under the Curve (AUC). However, this thesis has a large novelty factor as with the add-on it is possible to monitor other factors which were not possible previously and gather that data. In Milja's thesis only a single detector was available. [5]

Within the Turku PET Centre the delivery of radiowater has been the subject of ongoing investigation. Recently, a paper was published under the title *"Preliminary protocol for measuring the reproducibility and accuracy of flow values on digital PET/CT systems in [^{15}O] H2O myocardial perfusion imaging using a flow phantom"* (Siekkinen et al., 2024). In this publication a flow phantom was used to gain information about the radiowater administration process. This research utilised two different RWG systems *"Allowing us to also study the differences occurring due to two different bolus delivery systems".* As similar research continues to be carried out by Turku PET Centre (and possibly other radiowater users) a successful installation of this monitoring add-on could provide the researchers with more information regarding the operation of the radiowater delivery systems, RWGs. [6]

2 Aim of study and research questions

2.1 Aim of the study

The aim of this thesis is to successfully install the monitoring add-on to all existing radiowater generator (RWG) systems in Turku PET Centre and do preliminary analysis of the data that is provided by the monitoring add-on. The aim includes detailed documentation of this implementation process that is presented in this master's thesis. This includes the description of the functions and operation of the monitoring unit (installation, operation and data acquisition). This detailed documentation of this implementation can then be further processed into a technical note or user manual for this monitoring add-on in a separate (sub)project.

This thesis is not intended to be a release perquisite document for said add-on, but it can act as supporting material when Turku PET Centre and WASP research project participants are making decisions regarding the suitability of this system for pre-clinical research use. The aim is to provide an objective opinion of instrument suitability based on reliability and repeatability analysis.

2.2 Research questions

Based on the results obtained in this thesis, the goal is to be able to provide answers to the following research questions:

Research question one: *Does the monitoring add-on produce repeatable results?* If multiple identical measurements are produced with this add-on installed, is there a significant deviation within the acquired results (bolus curve characteristics, internal pressure and flow rate of components).

Research question two: *Is the data produced by the monitoring add-on comparable to the data produced by the RWG system?* Is the timing and bolus curve characteristic similar within these systems. This data can be further processed to establish a relation factor within the systems.

Research question three: *Is the monitoring add-on interchangeable among different RWG units?* In this thesis the monitoring add-on is planned to be installed parallel to three different RWG units that are used on site. These units are named after the PET/CT scanner that they designated to: Aino (Discovery MI, GE Healthcare), Vision (Biograph Vision 600, Siemens Healthineers) and Quadra (Biograph Vision Quadra, Siemens Healthineers). In this thesis the scanners and their designated

RWG units are referred to by their nicknames rather than make and model. This research question is evaluated regarding the variance within the results produced by different systems.

3 Background

This chapter contains all the relevant information regarding the systems and processes involved in this research project. This chapter describes the technical and physical characteristics of involved components with an adequate level of detail. In order to be able to interpret the results of this thesis, it is important to comprehend the processes described in this chapter.

3.1 Positron Emission Tomography

Positron Emission Tomography (PET) is a non-invasive nuclear medicine imaging procedure, that is used both in clinical and preclinical settings. In clinical use, PET is commonly used for neurological, cardiovascular and oncologic diagnostics. A significant value in PET imaging is the fact that it enables the visualisation of metabolic routes and processes, so that information about the target organs physiology and anatomy can be evaluated. This may enable the detection of abnormalities or the onset of a disease before anatomical changes related to the disease can be visualised with other imaging techniques such as Computed Tomography (CT) or Magnetic Resonance Imaging (MRI). PET is mostly combined with previously mentioned imaging methods CT or MRI to gain a more definitive overview of malignant tumours or other abnormalities. PET is a very frequently studied subject internationally and it has produced promising results in bettering the diagnostics of several diseases, most notably, Alzheimer's disease and coronary artery disease. [2]

PET principle of operation begins with the introduction of a radiotracer. Radiotracers are biological affinity molecules that contain a positron emitting component. Most commonly used radiotracer in PET is [^{18}F]-Fluorodeoxyglucose (FDG). In this radiotracer the biological affinity molecule is glucose and the positron emitting component is ^{18}F. Glucose is responsible for localisation of the molecule and ^{18}F is responsible for positron emission to the environment of the target area. In the case of FDG, the primary binding happens in the brain as glucose is an essential metabolic fuel for the brain. The positron emitting component of radiotracer undergoes positron decay, a process where a proton inside a radionuclide nucleus is converted into a neutron (n^0) while simultaneously releasing a positron (e^+ or β^+) and an electron neutrino (ν_e). This process can be simplified as the following:

$$Parent\ nucleus \rightarrow Daughter\ nucleus + Positron + electron\ neutrino$$

In the case of FDG the positron decay equation can be written out as:

$$^{18}_{9}F \rightarrow {}^{18}_{8}O + {}^{0}_{+1}\beta + {}^{0}_{0}\nu_e$$

Regarding PET the significant component of this decay process is the positron. Positrons are the antiparticles of electrons, meaning that they possess all the characteristics of an electron besides the opposite electric charge (electron e^- and positron e^+). This opposite electric charge causes the positron – electron interaction to result in particle annihilation. In particle annihilation the masses of the two colliding particles are converted into energy. Since the rest mass of both particles has an energy equivalent of 511 keV, the annihilation results in the energy release total of 1.022 MeV as the formation of two 511 keV gamma rays called annihilation photons. These photons exit the annihilation site at opposite propagating directions (approximately 180°). [7][8][9]

The annihilation photons produced in the process of particle annihilation are detected in PET systems through the detectors surrounding the imaging arch. Efficient detection of the photons requires the use of photodetectors. Previously PET systems have utilised Photomultiplier tubes (PMT's) as photodetectors, but modern systems are often based on Silicon photomultipliers (SiPM). It has been shown that SiPM are more reliable components regarding spatial, and timing resolution. These photodetectors are coupled with scintillators, which convert high-energy photons to light photons. These light photons are then amplified and registered by the photodetection components, which produce an electrical current proportional to the number of light photons detected. As the photons resulting from the particle annihilation process are emitted in opposite directions and the patient is surrounded with the detection system, oppositely aligned detectors will pick up the emissions simultaneously as depicted in Figure 1. As this particle annihilation process continues and the detectors keep getting multiple signals, a site of the particle annihilation can then be localised trough coincidence and time-of-flight calculations. The system is able to pinpoint the location of the annihilations and graph out a highly detailed image of the target site. [7][10]

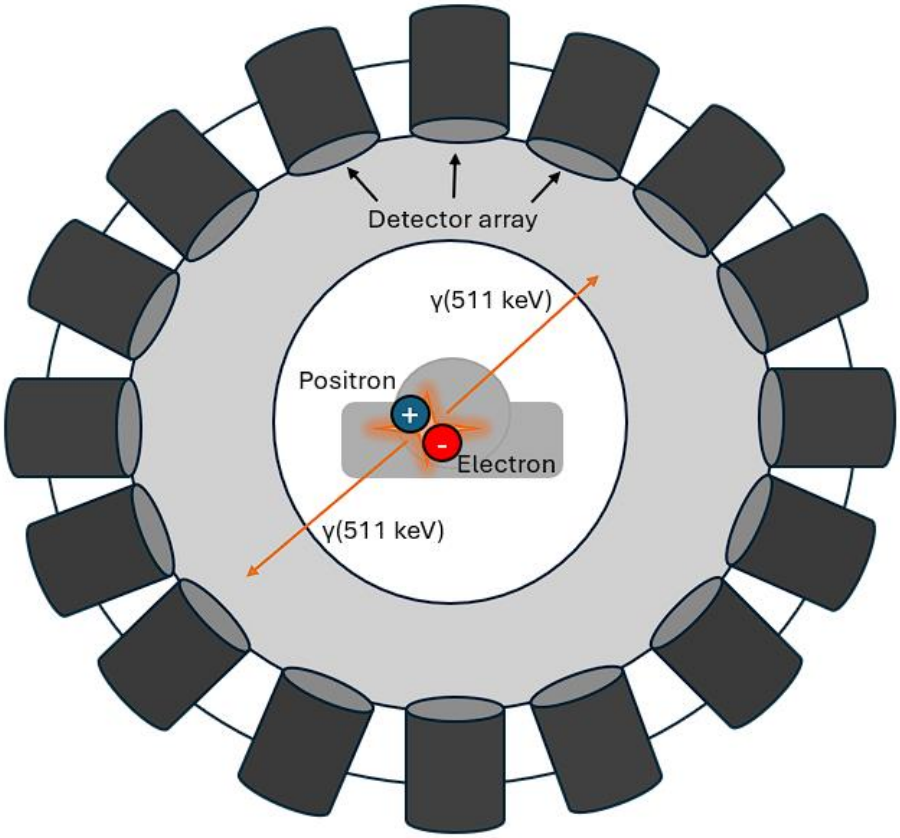

Figure 1. PET principle of operation (Modified from [11] Jiang et al.,2019)

3.2 Oxygen-15 labelled water as a radiotracer

Oxygen-15 is an unstable isotope of oxygen, which has a half-life of 122 seconds. In the decay process a positron is emitted. Regular water (H_2O) most commonly contains a stabile isotope of oxygen, ^{16}O. This stabile isotope of oxygen in water molecules can be replaced with its unstable, positron emitting counterpart to produce oxygen-15 labelled water [^{15}O] H2O, more commonly known as radiowater. The advantages that radiowater holds against most used PET tracers are most notably the short half-life, which results in smaller radiation doses to the patient. Another advantage that radiowater has, especially in perfusion imaging, is the fact that it possesses the characteristics of normal water. This means that it is freely diffusible in-vivo, which makes it theoretically a perfect tracer for whole body perfusion imaging procedures. In the case of Turku PET Centre, radiowater is currently used mainly for cardiovascular imaging, but in the future a new approach to radiowater use through total-body perfusion imaging is an interesting possibility for researchers within the facility. In order to facilitate these total-body radiowater studies, more information regarding the tracer, production of the tracer and the administration process needs to be obtained. [12][13]

In 2021 a publication was presented in the European Journal of Nuclear Medicine and Molecular Imaging (EJNMMI) titled *"EANM procedural guidelines for PET/CT quantitative myocardial perfusion imaging"* (Sciagrà et al., 2021). This publication was intended as a procedural guideline overview for cardiac PET and particularly quantitative myocardial perfusion PET. As the use of PET in myocardial perfusion procedures is increasing worldwide, the EANM Cardiovascular Committee found it suitable to describe the related subjects in this publication *"in order to establish an effective use of this modality and to help implementing it on a wider basis."* Radiowater is one of the radiotracers that is surveyed in this publication in detail and considered as *"The reference for non-invasive in vivo measurement of MBF because it is metabolically inert and essentially freely diffusible"*. In a chapter titled *"Pitfalls and artefacts"* the writer expresses that the problems associated with radiowater as a MBF tracer are related to for example patient motion or cardiovascular structure of the patient, but most notably (regarding this thesis) the problems are associated with the bolus delivery. Bolus delivery is a subject in radiowater administration that is constantly studied. [14]

Regarding the established clinical applications for radiowater, the most notable are the MBF studies as mentioned previously. Radiowater has proved to be very useful in diagnostics of cardiovascular conditions. It has been the method of choice in several MBF related studies. An example of one of the studies where radiowater was used to record cardiovascular functionality is a publication titled *"Myocardial blood flow in newly diagnosed breast cancer patients at rest and during exercise"* (Koivula et al., 2024). In this study radiowater bolus infusion method was used to compare the MBF of recently diagnosed breast cancer patients against a healthy control group. Although MBF can be characterised in multiple ways, such as echocardiography, PET seems to have established itself as the standard method for total MBF measurements. The radiotracers used vary according to imaging site production capabilities and legislation, but the competition for leading radiotracers for MBF studies seems to be between ^{15}O and ^{82}Rb. According to literature, ^{82}Rb seems to be more widely used in North America in myocardial stress perfusion studies. As stated before, the used tracer is often dependent on the legislation and the production capabilities within the imaging site. ^{82}Rb is a generator-produced radiotracer and requires special instrumentation within the facility to utilise in MBF studies. A very beneficial characteristic that ^{82}Rb holds over ^{15}O as a radiotracer is the shorter half-life. In a publication titled *"Generator-produced rubidium-82 positron emission tomography myocardial perfusion imaging—From basic aspects to clinical applications"* (Yoshinaga et al., 2010) it is stated that "Among PET perfusion tracers, ^{82}Rb has the shortest physical half-life with 76s". [15][16][17]

Total-body PET imaging has already been the subject of study within Turku PET Centre to an extent. This is the product of many factors, but most notably it is related to imaging instrumentation development and specifically scanners enabling long axial field of view. This allows the researchers to simultaneously visualise all organ functions and their interactions. This is demonstrated in an article by Turku PET Centre titled: *"Quantitative Perfusion Imaging with Total-Body PET"*. (Knuuti et al., 2023). In this publication the instrumentation, radiotracers and data acquisition handling methods were evaluated regarding suitability for total-body quantitative perfusion imaging procedures. In the summary of the publication the following statement is made: *"^{15}O-water as a biologically inert and freely diffusible tracer is likely the tracer of choice for perfusion quantitation."*. As demonstrated by this publication, it is apparent that radiowater has potential to be utilised in applications that have not yet established their position in clinical diagnostic settings. [18]

3.2.1 Oxygen-15 production in Turku PET Centre

Multiple radionuclides including Oxygen-15 are produced for medical purposes through particle acceleration. There are various types of particle acceleration devices, but for medical radioisotope production a particle accelerator type called a cyclotron is often utilised. This is also the case in Turku PET Centre. The working principle of the cyclotron in comprehensive detail is not relevant regarding this thesis. The simplified description of cyclotron working principle can be described as follows: Two oppositely positioned semicircle hollow halves, called "dees" are mounted to each other to create a circular structure, which is then encased in a vacuum chamber. Inside these halves an alternating polarity electric field is established. Due to a magnetic field surrounding the structure, the introduced particles will move in a spiral pattern. An ion source to be accelerated is introduced into the middle of the system. By alternating the polarity of the electric field this source can be accelerated in a circular, expanding radius pattern, until it reaches the exit channel in the outer layer. This exit channel allows the source particle to enter a bombardment chamber, where it collides with the target in high speed to alter the target's atomic composition, thus creating a new isotope, for example ^{15}O. The working principle of the cyclotron is depicted in Figure 2. [19]

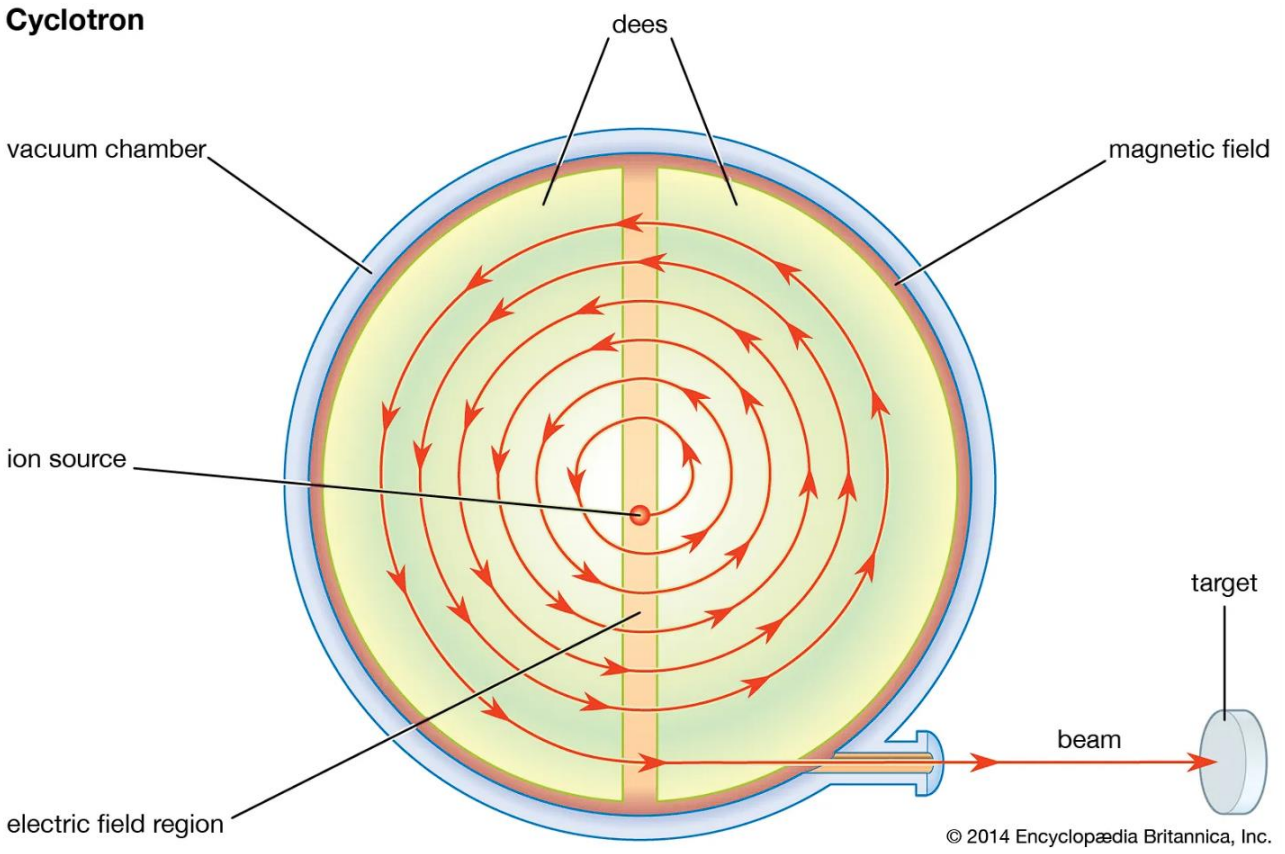

Figure 2. Plan view of the cyclotron, Encyclopaedia Britannica, Inc. [19]

Depending on the target radioisotope, the composition of the bombarded target varies. Most commonly, ^{15}O is produced through deuteron bombardment of nitrogen gas target, in which a ^{15}O nucleus and a neutron is produced via the $^{14}N(d,n)^{15}O$ reaction. In this case, the bombarded target gas is composed of 99% nitrogen (N_2) and 1% oxygen (O_2). There are alternative routes to this reaction, which involve different types of bombardment protocols or targets, but the key aspect is that in all ^{15}O production procedures the cyclotron end product is the $^{15}O_2$ gas. [19][20]

The produced $^{15}O_2$ still requires some processing before it is suitable for administration to patients in radiowater infusion studies. As mentioned previously, ^{15}O is most commonly administered intravenously to patients in its radiowater form [^{15}O] H_2O. Alternatively, the composition of the target gas can be 99% N_2 and 1% CO_2. This results in the end product [^{15}O] CO_2 for gaseous administration, in which it is converted to radiowater trough inhalation. But in the intravenous radiowater administration, the $^{15}O_2$ gas needs to be converted into radioactive water vapour in high temperatures. This process is described in chapter 3.3. [21]

3.3 Radiowater generator working principle

The radiowater generator system encompasses the Hidex RWG Furnace System and the Hidex RWG system. The working principle of the radiowater generator system is illustrated in Figure 3. To uphold market integrity and respect the manufacturer's interests, certain components have been omitted from this schematic. The exact composition and physical factors, however, are not considered as essential information regarding the general working principle of the system.

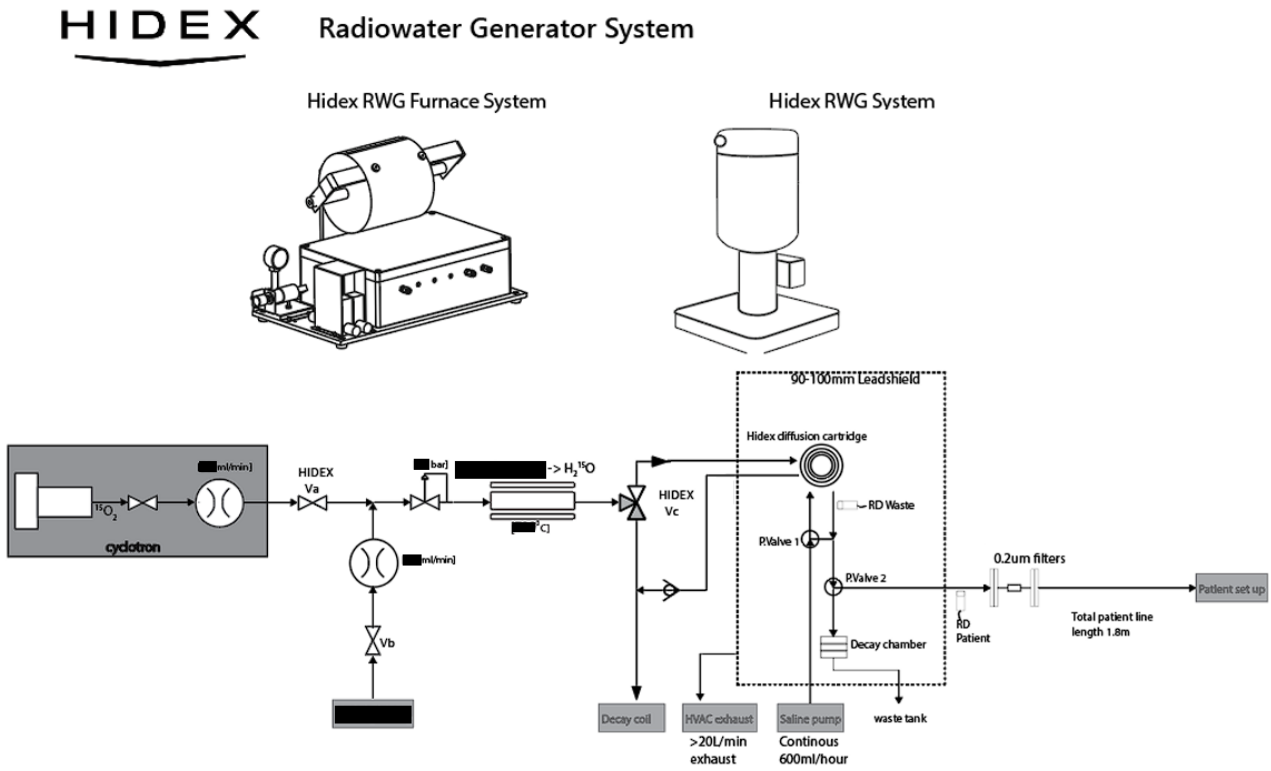

Figure 3. Radiowater Generator System, Hidex Oy [22]

As mentioned in chapter 3.2.1 the radioactive water vapour ($[^{15}O]H_2O$) is the desired product that is utilised in radiowater production. This radioactive water vapour is acquired by exposing the cyclotron end product to high temperatures alongside carrier gases in the Hidex RWG Furnace System. This radioactive water vapour is then transported to the bedside generator. The bedside generator is a lead shielded structure, which houses the diffusion cartridge. The bedside generator is connected to the peristatic pump and infusion system, which enables the introduction of saline into the diffusion cartridge. In this diffusion cartridge, the radioactive water vapour diffuses through semi-permeable membrane into the saline, resulting in the formation of the injectable radiotracer. [21]

The RWG system houses the previously mentioned diffusion chamber. The diffusion chamber houses a diffusion kit, which is a circular membrane "cartridge" that has designated inlets and outlets for different components. These outlets allow the movement of gas and saline within the cartridge and control when components are either taken in, or excreted either to waste line for disposure, or to the patient line for intravenous administration. The outgoing lines to "patient" or "waste" are monitored by fibre optic scintillator detectors (described in detail in chapter 3.5) so that the user is given the information regarding how much radioactivity has passed through each line. These lines are controlled by air compression pistons, which can clamp the lines shut or leave them open, depending on the stage of the administration process. [22]

3.4 Radiowater administration process

The radiowater administration process is carried out from within the control room of the imaging procedure area. The process is controlled through RWG console user interface to which the operator inputs parameters and initiates the administration process. Administration protocols can vary depending on the instrumentation available within the site. The radiowater administration process can be carried out as a continuous infusion, in which the patient is continuously infused with the radiotracer, or bolus infusion, in which the radiotracer is administered as a more concentrated single dose within a shorter period of time (max. 15s.). The bolus infusion protocol is used in Turku PET Centre, and therefore that is the protocol that is described and used in this thesis.

The bolus administration process has different stages, which include the following:

Collection and preflush: RWG collects radioactivity within the diffusion cartridge for 120 seconds and prepares the bolus for patient infusion. Simultaneously the system is infusing the patient with saline to ensure that a proper intravenous administration route is established.

Infusion: The contents of the diffusion cartridge are released into the infusion line, and the collected bolus travels through the infusion site into the patient. The infusion can be carried out either as an all-pass run or as a "cut" run. The calibration all-pass runs are carried out in Turku PET Centre daily to ensure that the system is properly calibrated. In the all-pass run, the infusion lasts 15 seconds, and the bolus is produced into a vial, that is then measured using a dose calibrator and half-life is corrected to establish a calibration factor of the system. The cut run means that the amount of radiotracer exiting the RWG is monitored in real time, and the infusion is stopped as the desired amount of radiotracer has exited the diffusion chamber. This is monitored by the RWG Patient detector, mounted in the infusion line right outside the generator. In this thesis, the data sets include 6 all-pass runs and 4 cut

runs from each system to gain an understanding of the functionality of both of these bolus administration types.

Flush: After the infusion is completed, the valve configuration in the diffusion chamber is once again altered, and the infusion line bypasses the cartridge, only feeding saline solution to the line. This is done to flush out any remaining radioactive material. [22]

4 Materials and methods

4.1 Monitoring add-on composition and working principles

The monitoring add-on is constructed upon Beckhoff PLC (Programmable Logic Controller). It consists of two modules and measurement related components. User can access the logic of this monitoring add-on through any PC system that supports remote desktop access through ethernet connection. This chapter includes the composition of the monitoring add-on and details the functionality and placement of the components that are relevant regarding data acquisition. Diagram of the components are presented in Figure 4 and measurement related components, and their functionality and placement are detailed in Table 1.

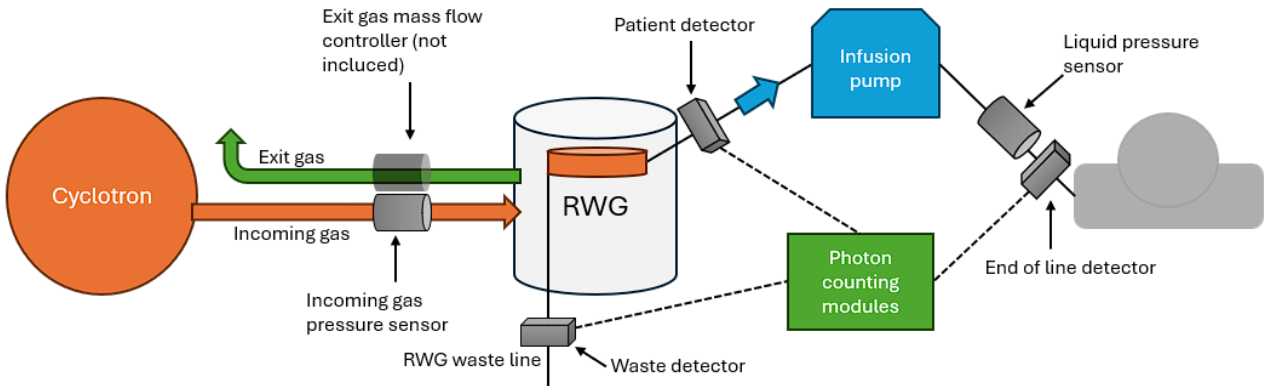

Figure 4. Diagram of the monitoring add-on components

Table 1. Monitoring add-on components

Component type	Make and model	Function and location of the component in the system
Liquid pressure sensor	Bronkhorst EL-PRESS P-532C	Monitors the liquid pressure in the patient line. Installed between the peristatic pump and the infusion point
Gas pressure sensor	Bronkhorst EL-PRESS P-502C	Monitors the gas pressure of incoming gas from the cyclotron to the RWG. Installed in the cyclotron-RWG target gas line
Gas mass flow controller	Bronkhorst EL-FLOW Select F-201CV	Monitors the volume of waste gas exiting the RWG to waste decay line. Installed in the RWG-gas exit waste line (logic existing in the monitoring add-on, not installed currently due to component unavailability)
Fibre optic scintillator clip	Hidex B-PET-20001473	Scintillator produces pulses from radioactive material passing through patient tubing which are delivered through fibre optic line to PMT modules. Patient detector and waste detector are installed parallel to the RWG detectors, patient in the exit patient line and waste inside the cartridge waste loop. The end of line detector is installed at the infusion point next to the needle. (Structure displayed in Figure 4.)
Photon counting module	Hamamatsu H11890-210-RS	Records and processes the pulses obtained from fibre optic line. Located within the add-on module and connected to fibre optic scintillator clip via fibre optic cable.

The functionality of the fibre optic scintillator clips is an essential factor in the monitoring of radioactive components within the system. Structure of the fibre optic scintillator clip is depicted in Figure 5. The existing RWG system utilises the same fibre optic scintillator component. The principle of operation is as follows: The fibre optic scintillator clips are mounted to the patient tubing in predefined locations. As the radioactive material (radiowater) moves inside the patient tubing, it constantly emits ionising radiation. As the radiowater passes a fibre optic scintillator clip, mounted around the patient tubing, the radiation causes the scintillator insert to absorb the energy and elevate to an excited state. This results in the emission of photons as the scintillator's excitation state deteriorates. These photons are then picked up by the fibre optic line and transported to the photon counting modules inside the add-on for processing. This allows the acquisition of activity curves in different states of the radiowater administration process. [23]

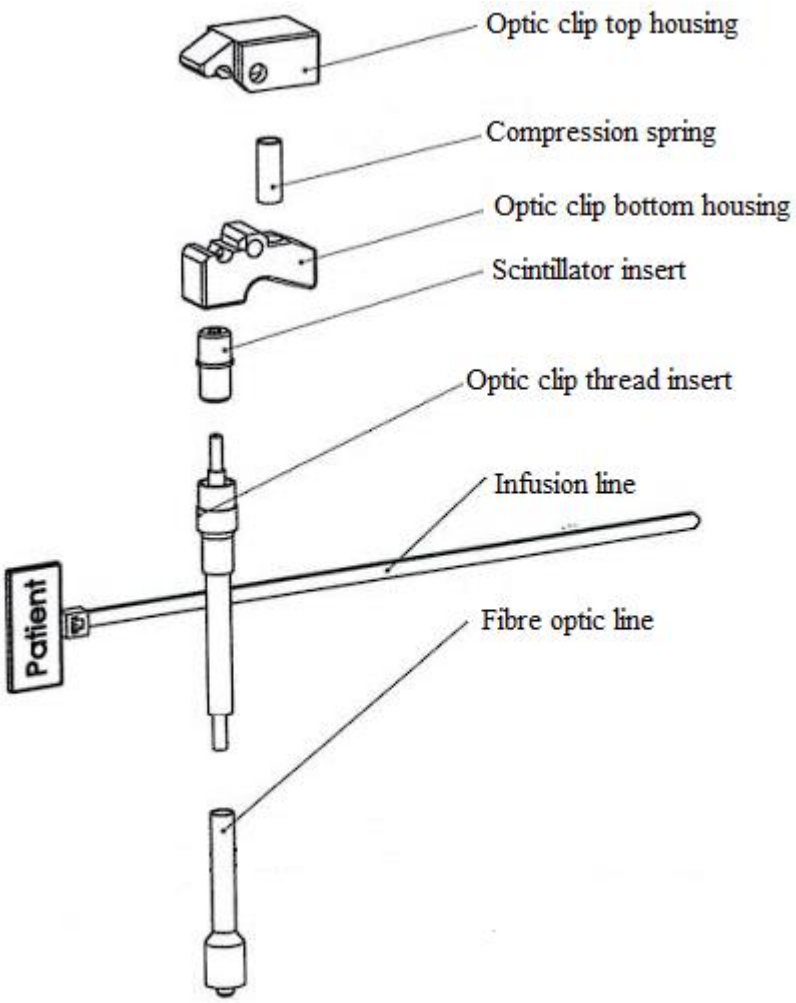

Figure 5. Assembly drawing of the fibre optic scintillator clip, Hidex Oy [24].

The system encompasses three different fibre optic scintillator clips which respond to different photon counter activity curves. The positions and correspondence of each fibre optic-photon counter pairs are as follows:

Photon counter 1 – Mounted directly next to the RWG patient detector, outside the lead shield construction. Produces an activity curve of the material leaving the RWG diffusion chamber in patient infusion state of the procedure.

Photon counter 2 – Mounted next to the needle in infusion point. Produces an activity curve of the material that is excreted from the cannula.

Photon counter 3. – Mounted next to the RWG waste detector, inside the lead shield construction. Produces an activity curve of the material directed to the waste line after the patient infusion state of the procedure.

In order to be able to operate the monitoring add-on, a TwinCAT PLC control software-based user interface (UI) is constructed. Connection to this UI is established through windows remote desktop access. Within this UI the status of each monitoring component is displayed, and the user can adjust the functionality of the add-on, such as define sampling rates depicted in Figure 6.

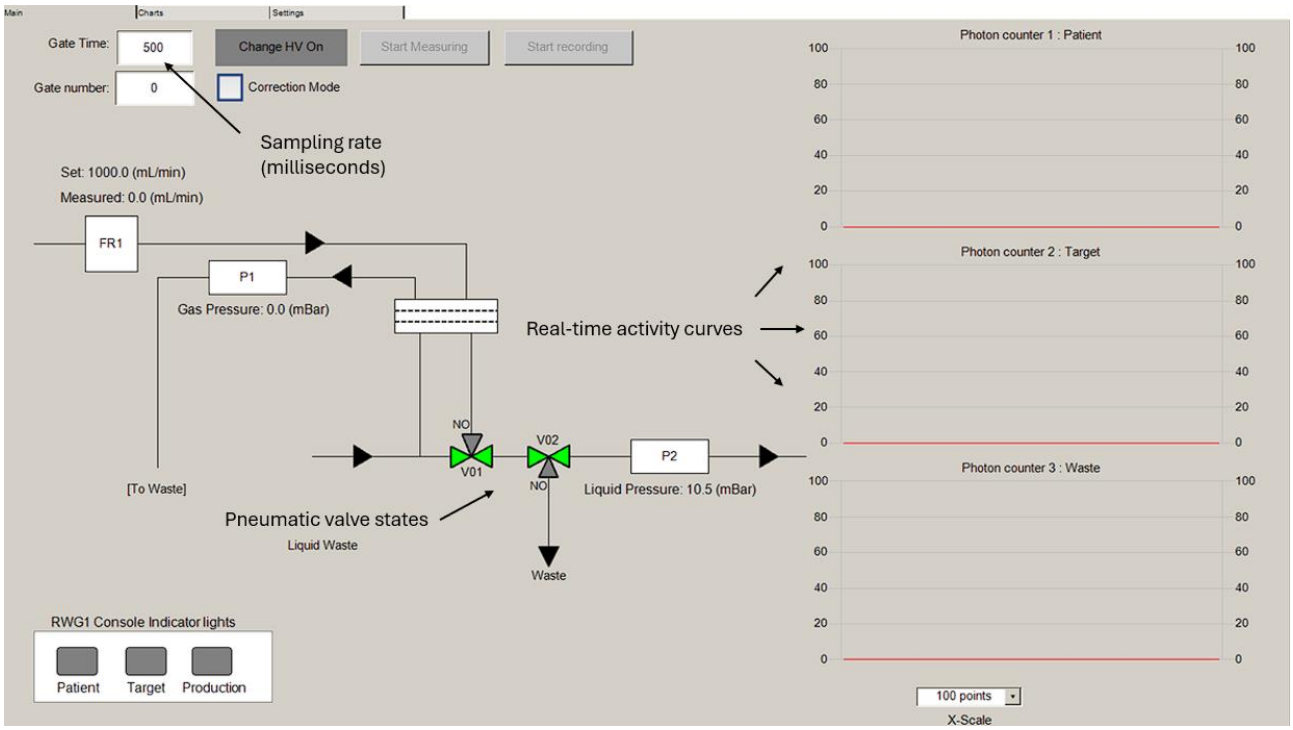

Figure 6. Monitoring add-on UI main view.

When the monitoring add-on recording status is toggled on, it begins to write the data files to the internal computer, from which the .csv-based measurement data can be accessed. From the monitoring add-on UI, the real time curves for all monitored components can be accessed through the "Charts" view depicted in Figure 7.

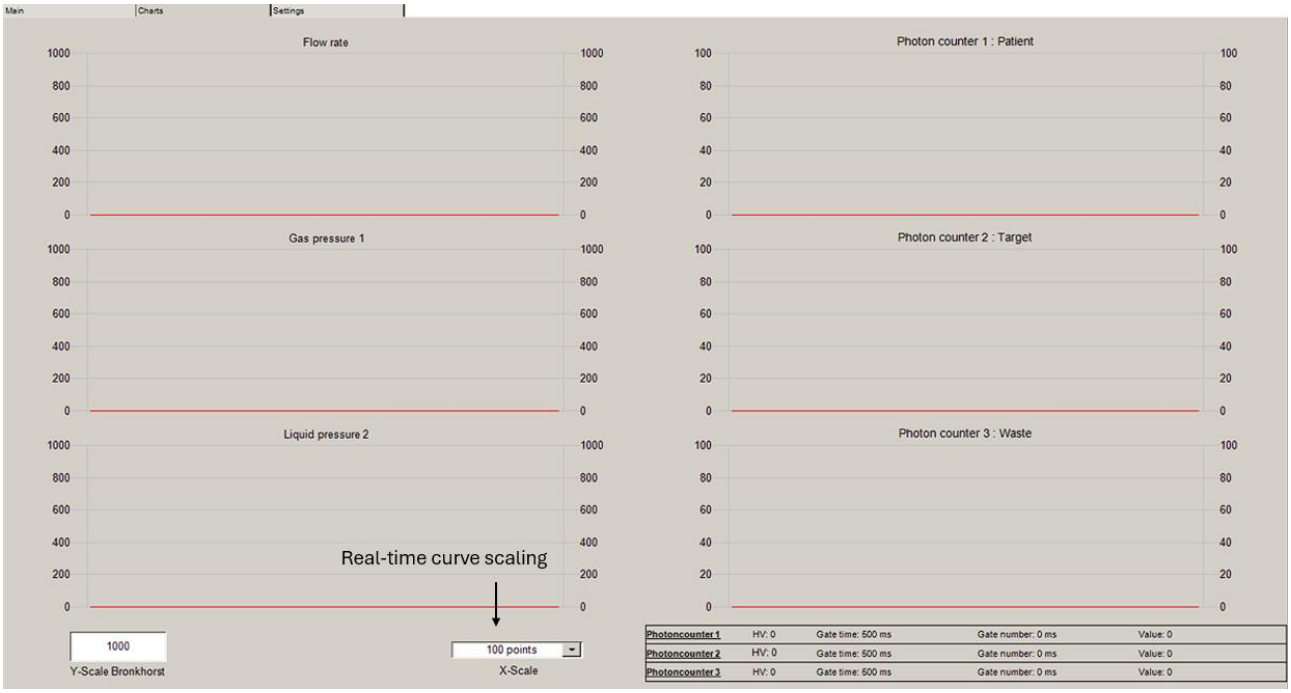

Figure 7. Monitoring add-on UI Charts view.

The "charts" -view displays all monitored components according to the scaling set by the user. This enables the user to monitor changes within the system in real-time, rather than having to process the recorded data in external software.

4.2 Monitoring add-on placement and detector orientation

The monitoring add-on consists of two modules, which house the measurements electronics and related components. Module 1 is the PLC controller. This module contains the internal computer and is responsible for adjusting measurement parameters, enabling recording and connections to RWG console and the PC used for UI display and data extraction. Module 2 is the PLC signal box. This houses all the PMT modules and measurement related electronics. The pressure lines and fibre optic cables are connected to this module. Being a non-fixed system, the modules can be placed as desired, but it has been found suitable to place the modules as depicted in Figure 8.

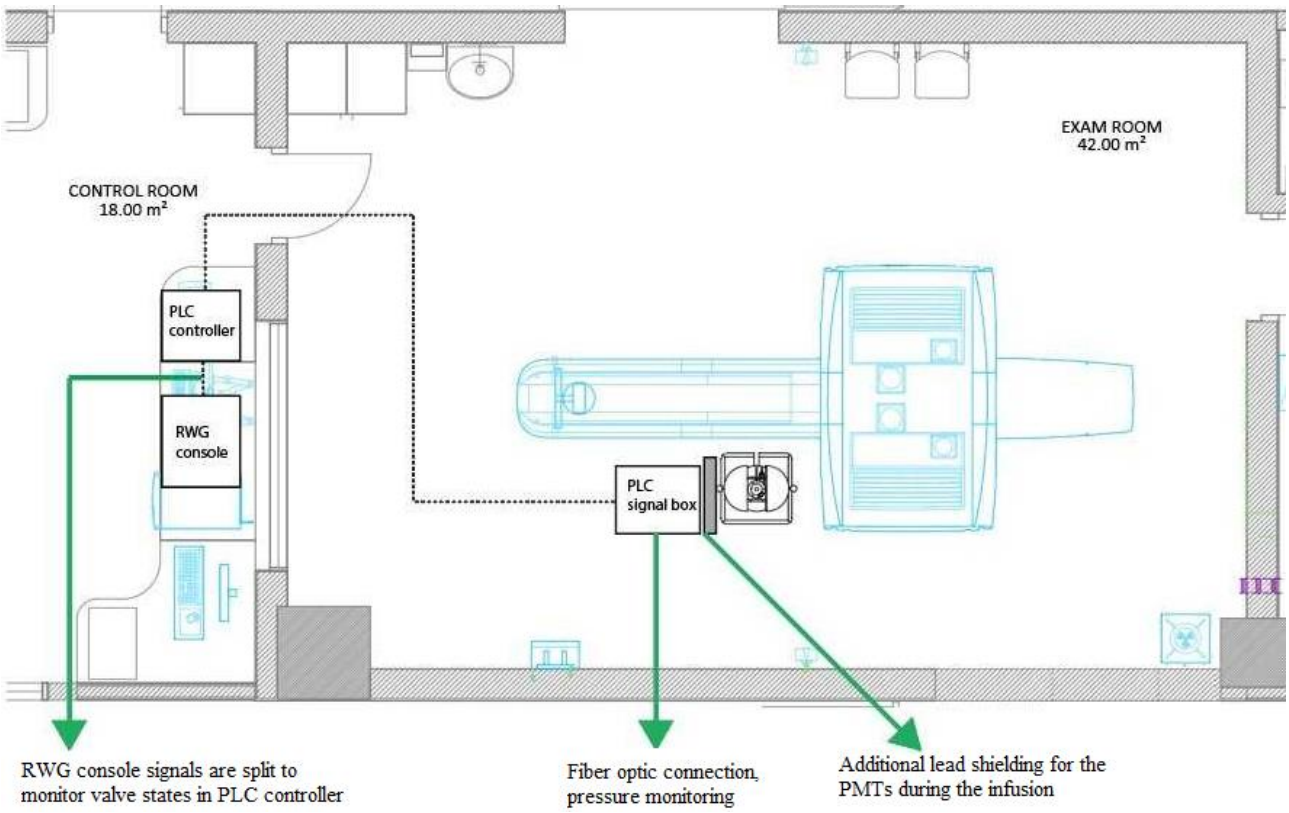

Figure 8. System layout in operation, Hidex Oy [23].

The signal box is located inside the exam room in order to minimise the cable lengths for all measurement electronics. The signal box is connected to the controller module, which is located in the control room along with the RWG console and control PC.

Due to the sensitive nature of the PMT modules, it has been found beneficial that the signal box and measurement electronics are sheltered using a lead block array or (semi)permanent lead structures within the operation room (such as the RWG lead shield) to minimise interference originating from the radioactive infusion lines. The monitoring add-on modules installed according to the operation layout are depicted in Figures 9 and 10.

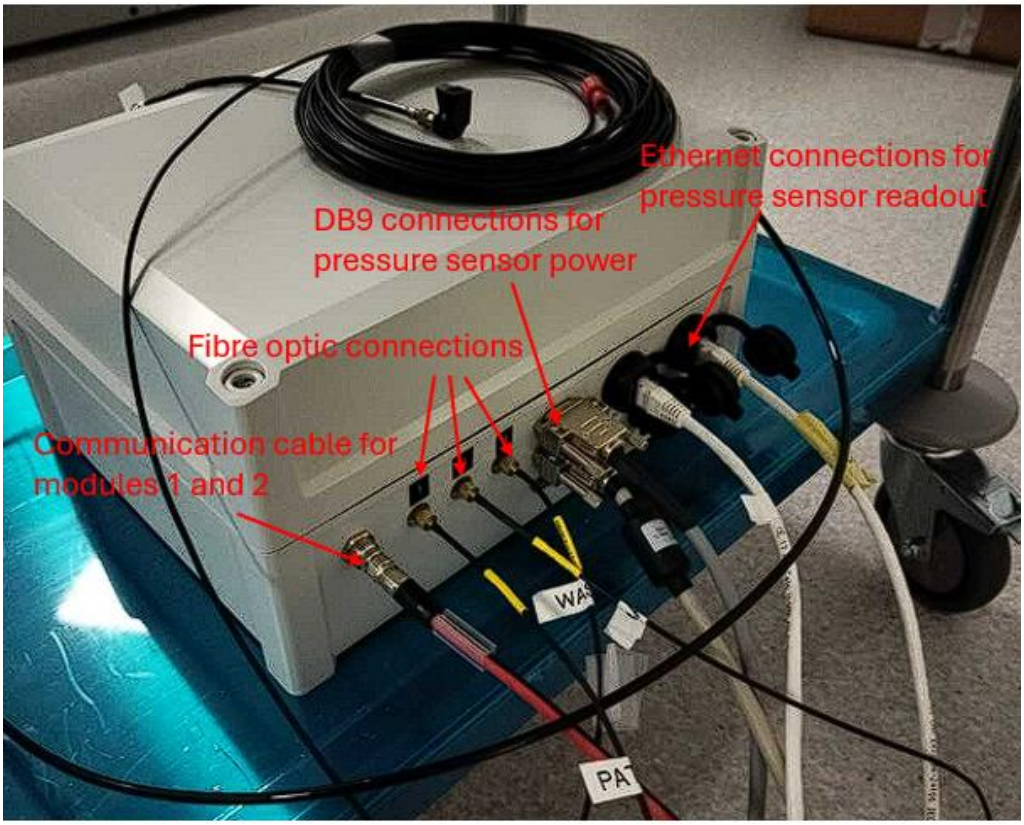

Figure 9. PLC signal module in examination room.

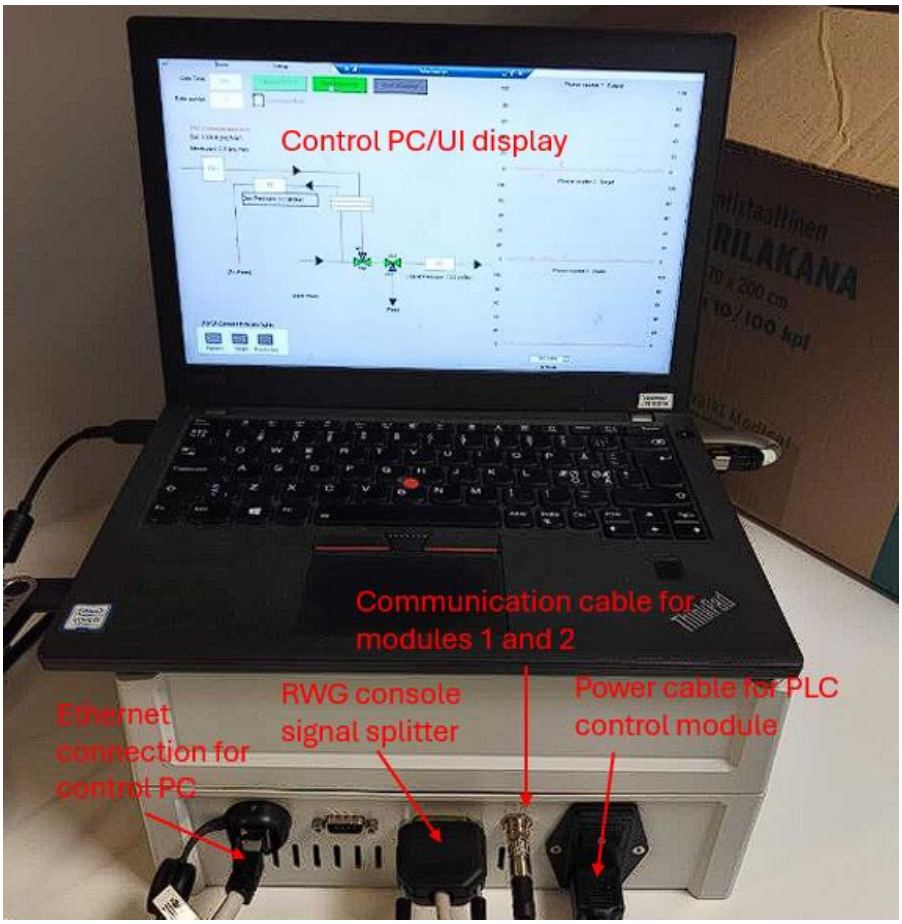

Figure 10. PLC controller module in control room.

In testing procedures, the radiotracer infusion is produced into a vial. This vial simulates a patient as the site where the radiowater exits the system. Setup of the infusion vial is depicted in Figure 11.

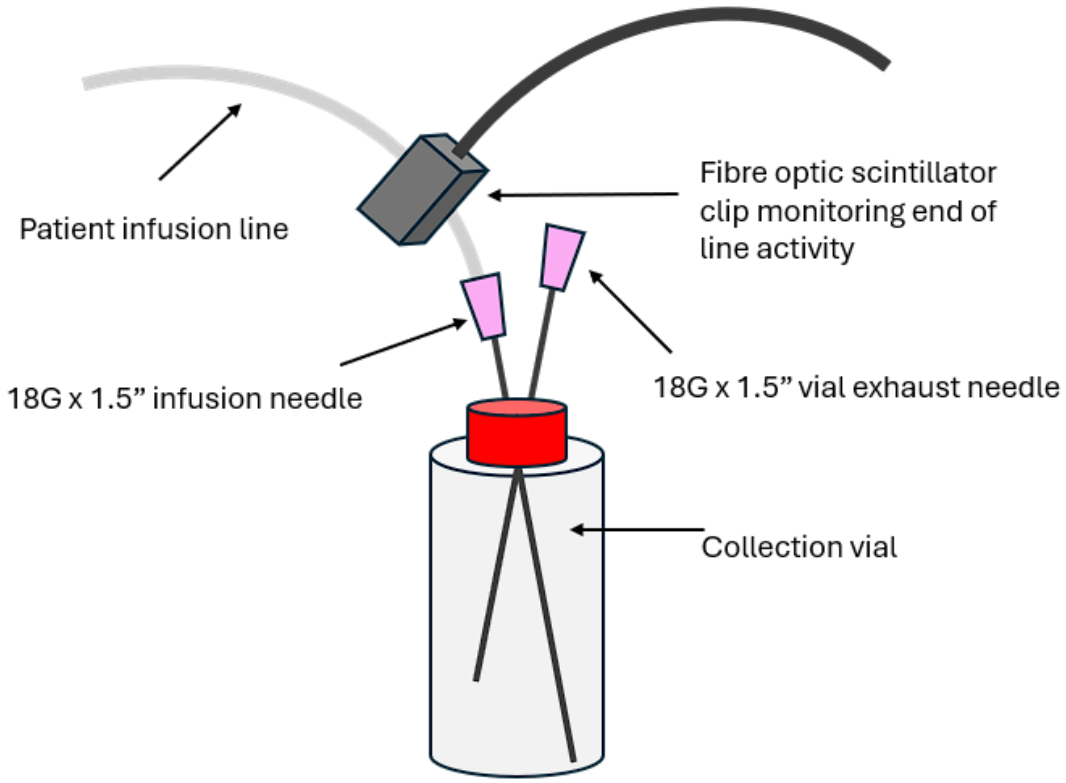

Figure 11. Infusion vial setup.

The infusion vial setup consists of a collection vial that has two needles inserted into it. One of the needles is for the infusion, and through that needle the intravenous access to the patient is established in patient procedures. The other needle is specific to this type of vial infusion setup and acts as the exhaust needle to ensure that no pressure is building up inside the membrane sealed vial. Pressure buildup or any pressure variance could disrupt the flow of radiowater to the vial. Fibre optic scintillator clip (described in chapter 3.5) is connected to the patient infusion line. The reading of this detector is responsible for producing the end of patient line activity curve. Due to the previously mentioned phenomenon where radioactive material passing through non-shielded infusion lines affects the sensitive measurement electronics, the vial setup is encapsulated in a lead cylinder, and the exposed infusion lines are fixed behind the RWG lead shield structure. This is done to minimise the effects that an exposed radiation source may have on the measurement electronics located near to it. The vial setup is presented in Figure 12 below.

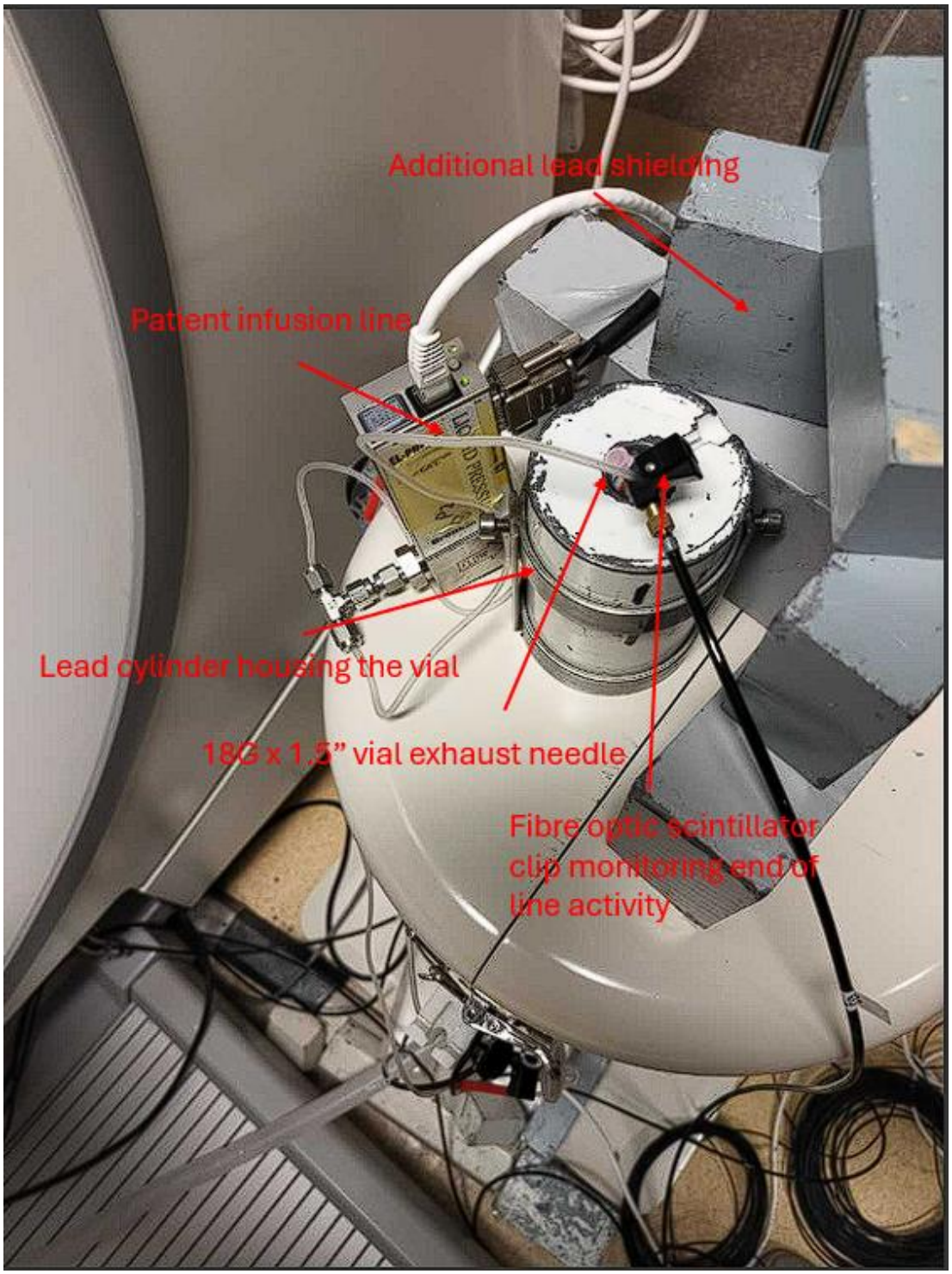

Figure 12. Sheltered infusion vial setup.

4.3 Data acquisition and pre-processing

The data acquired from the monitoring add-on is extracted through remote desktop connection in .csv format. In this raw data form, there are separate columns for each recorded parameter. The recorded parameters include the following: patient PMT, end of line PMT, waste line PMT, gas pressure and liquid pressure. The raw data file contains a value for each of these values according to set sampling rate. In this dataset, the sampling rate was set at 500 milliseconds as that is equal to the RWG default sampling rate. The values from each of the PMT columns were then processed using Python based calculator to plot the activity curves, AUC and FWHM. The used calculator script evaluates the FWHM and AUC from channels 240 to 490 as this is the expected range that the bolus will be recorded by the detectors (Appendix 1). This Python script plots the activity curves according to Simpson's rule, which is a numerical integration correction factor that is more accurate than trapezoidal rule, as it approximates the curve as a piecewise quadratic (parabolic) function between the points. All of the raw data columns for previously mentioned parameters along with the activity curves and their FWHM and AUC values were then extracted to a master dataset that contains all performed measurements from each RWG setup, Aino, Quadra, and Vision. These datasets containing the processed curve characteristics are then evaluated regarding repeatability, monitoring add-on data against RWG data and all generators monitoring add-on data compiled. [24]

4.4 Conducted measurements

This chapter describes the measurements that were conducted using the monitoring add-on and the reasoning for each value monitored. Measurements were conducted using three different RWG systems, Aino, Vision and Quadra within a timespan of three months. The sampling rate for all measurements was set at 500 millisecond intervals, as this is the same timescale used by the RWG console. This enables the comparison of the peak timing versus the RWG. All systems were tested with six all-pass protocols and 4 cut protocols. The operating principles of both all-pass and cut are explained in detail in chapter 3.4. During these test runs the following parameters were recorded and they are presented in the results chapter:

1. Patient line activity curves for six all-pass runs and four cut runs. This is done to demonstrate the system's capability to produce repeatable results from the patient line detector and to compare the variance within RWG generator systems.

2. End of line activity curves for six all-pass runs and four cut runs. This is done to demonstrate the system's capability to produce repeatable results from the end of line detector and to compare the variance within RWG generator systems.
3. Waste line activity curves for six all-pass runs and four cut runs. This is done to demonstrate the system's capability to produce repeatable results from the waste line detector and to compare the variance within RWG generator systems.
4. Incoming gas line pressure for six all-pass runs and four cut runs. This is done to demonstrate the stability within the system and to record potential changes and gas pressure baseline within different RWG systems.
5. Liquid pressure for six all-pass runs and four cut runs. This is done to demonstrate stability within the system and to record potential changes and liquid pressure changes within different RWG systems.
6. Monitoring add-on detector activity curve analysis for all detectors (patient, end of line, and waste) demonstrating curve width regarding FWHM and area regarding AUC. This is done to record curve characteristics such as peak timing or changes in the curve width. Demonstrates system repeatability and compares the potential differences in curve characteristics within different RWG units.
7. RWG curve analysis regarding FWHM, AUC, and bolus peak timing. This is done to compare the boluses recorded with the monitoring add-on against the boluses recorded with the RWG system. The focus on this analysis is to compare the timing of the bolus peak, which can be seen from the maximum channel value.

5 Results

This chapter includes the monitoring add-on data and RWG console data from each of the three systems used, Aino, Vision and Quadra. Each chapter contains the relevant data from all three systems used along with an explanation of the recorded values and potential abnormalities related to each section. In detector activity curves, the Y-axis corresponds to the detected radioactive emission events by the target detector at given timepoint as Counts per Second (CPS). In all recorded measurements X-axis corresponds to the channel timepoint. As the sampling rate for these measurements was set at 500 milliseconds, each channel represents an interval of half a second.

5.1 Patient detector activity curves

Below is presented the patient detector activity curves for all three systems in six all-pass runs (run 1-6) and four cut runs (run 7-10). It is notable that the peristatic pump used for Aino all-pass runs 1-5 had some unknown issue relating to too small flow values. The data from Vision run number 6 was lost due to circumstances not related to the monitoring add-on.

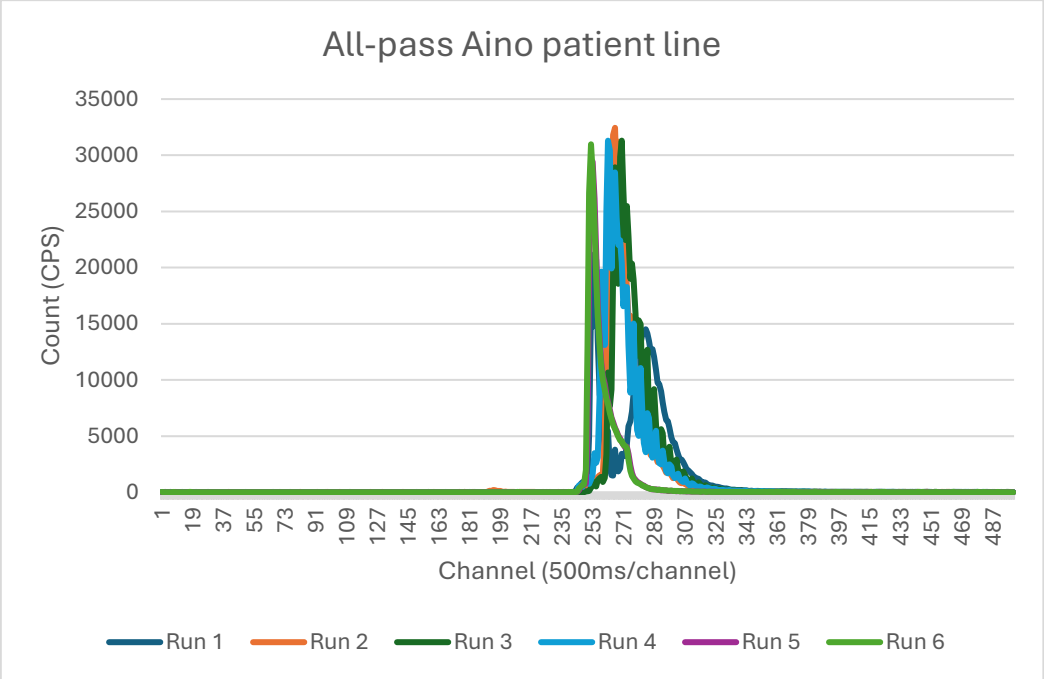

Figure 13. Aino all-pass patient line.

Figure 13 depicts the bolus curve series recorded by the patient detector. The infusion begins from channel 240 which causes the detector reading to increase, and after finishing the infusion the detector reading returns to the base level. Run six is considered to be more of a normal run, and the runs

conducted before that have significant variance in both peak position and shape due to the previously mentioned peristatic pump issues.

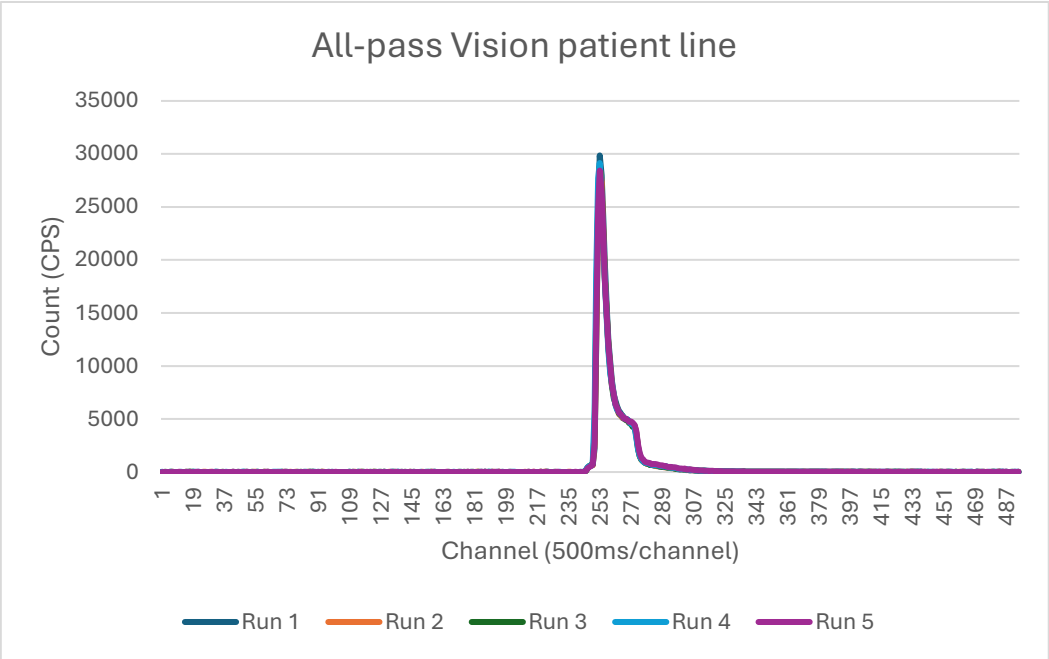

Figure 14. Vision all-pass patient line.

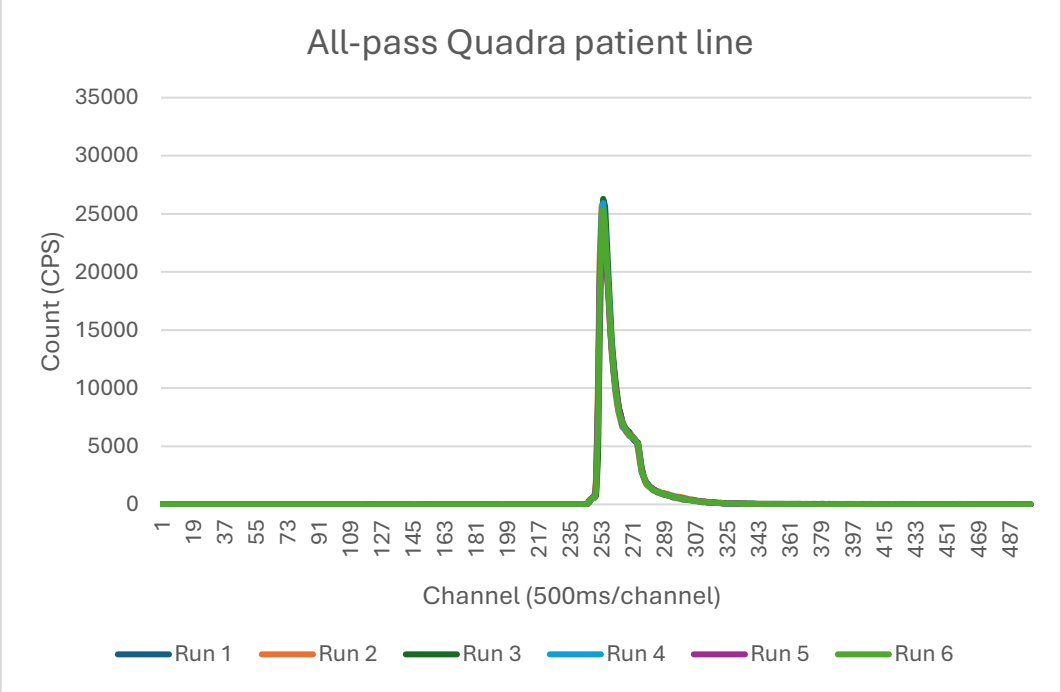

Figure 15. Quadra all-pass patient line.

Figures 14 and 15 demonstrate an all-pass bolus curve series recorded by their respective patient detectors. The infusion begins in channel 240 which causes the detector reading to peak, and then the

infusion stops after a set timepoint (All-pass run) which causes the detector reading to return to the base level around the channel 307.

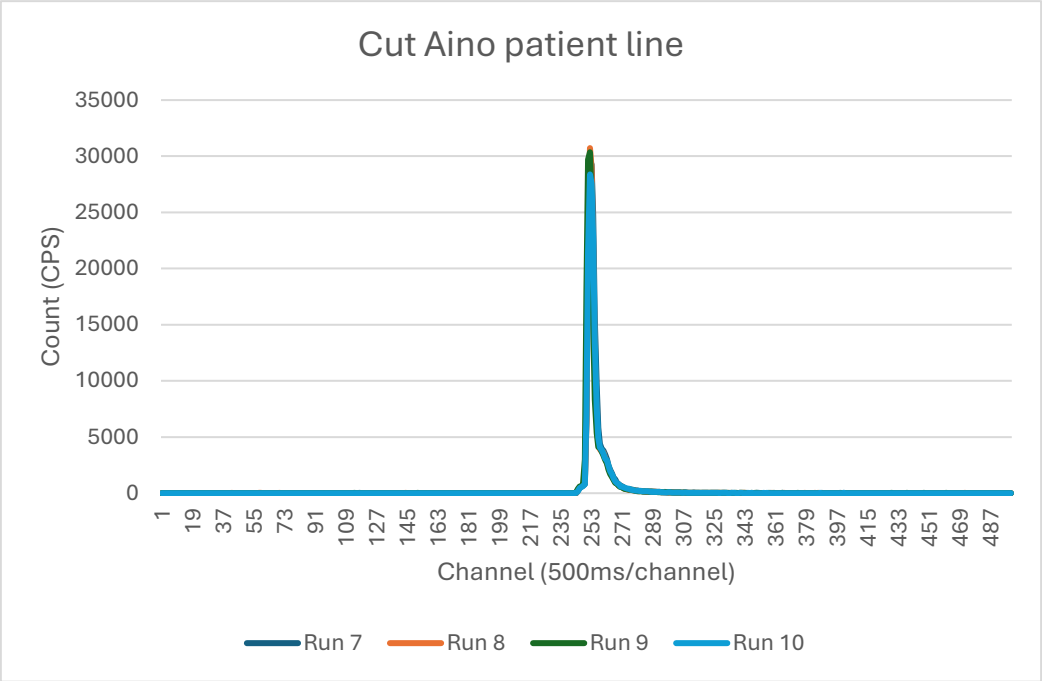

Figure 16. Aino cut patient line.

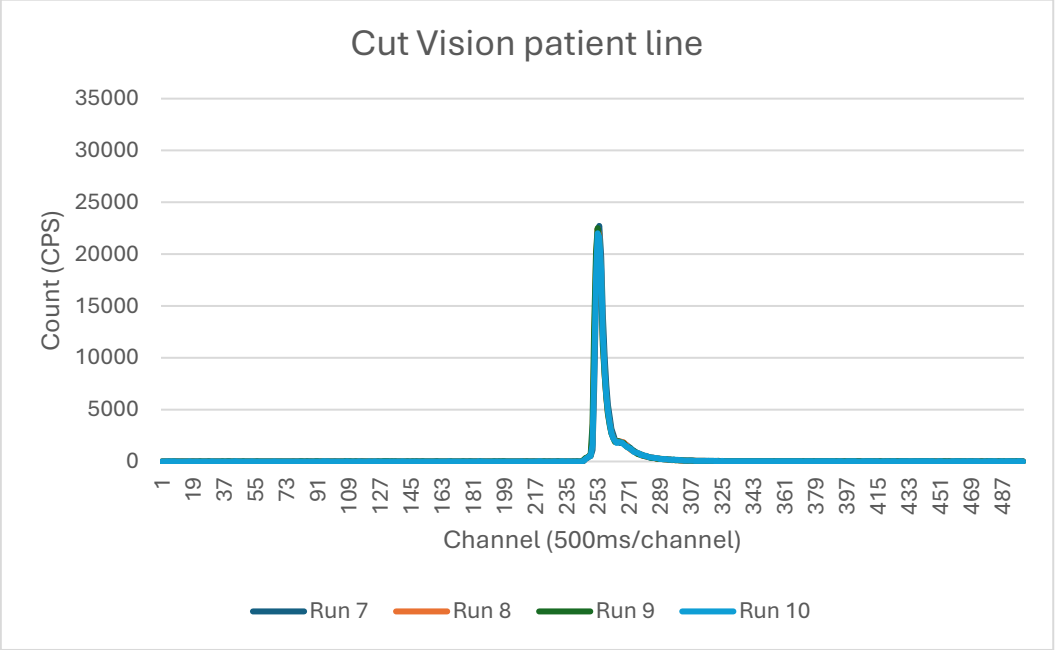

Figure 17. Vision cut patient line.

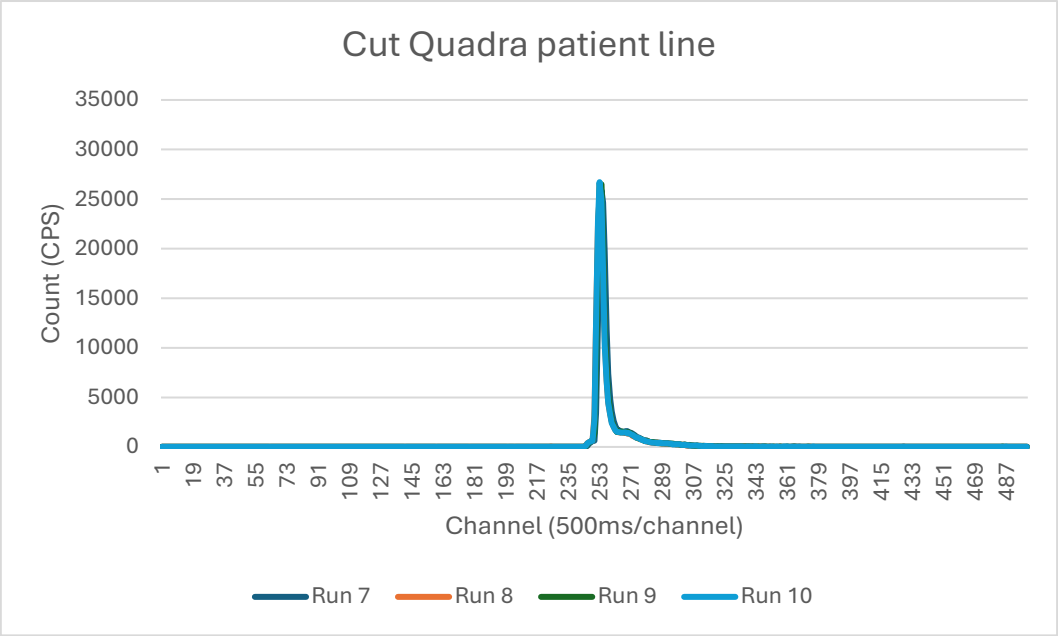

Figure 18. Quadra cut patient line.

Figures 16-18 demonstrate a cut bolus curve series recorded by their respective patient detectors. The infusion begins at channel 240 and after the required amount of radioactivity has passed the RWG patient detector (cut run) the infusion stops which causes the detector to return to the base level.

5.2 End of line detector activity curves

Below is presented the end of patient line detector (located at the infusion point) activity curves for all three systems in six all-pass runs (run 1-6) and four cut runs (run 7-10). It is notable that the peristatic pump used for Aino all-pass runs 1-5 had some unknown issue relating to too small flow values. The data from Vision run number 6 was lost due to circumstances not related to the monitoring add-on.

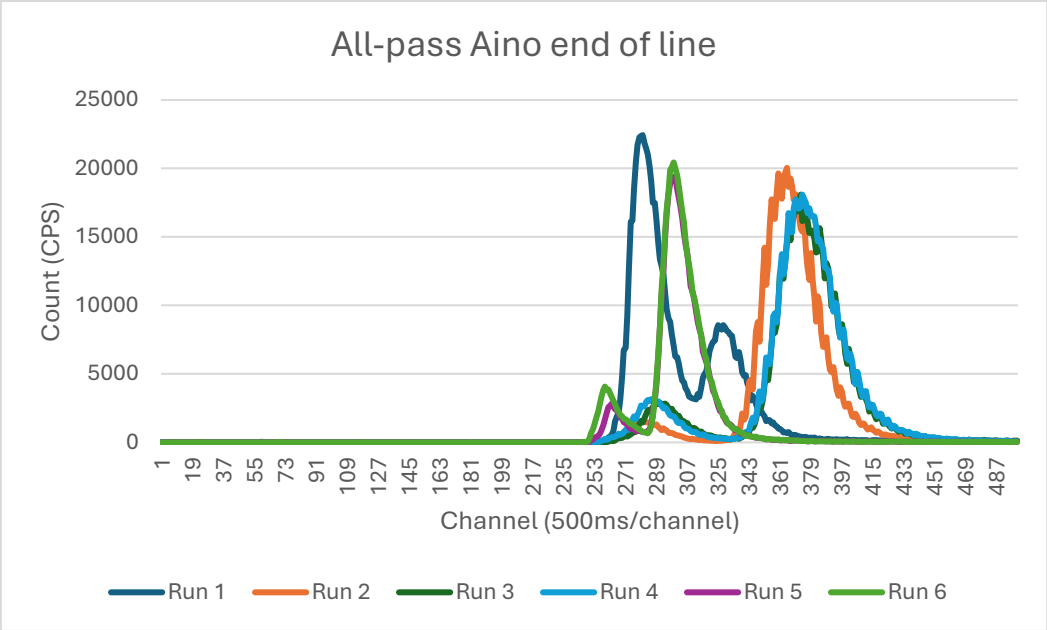

Figure 19. Aino all-pass end of line.

Figure 19 contains a bolus curve series for all-pass protocols recorded by Aino end of line detector. Variability in the peak position and shape is resulting from the peristatic pump which is previously described in chapter 5.1.

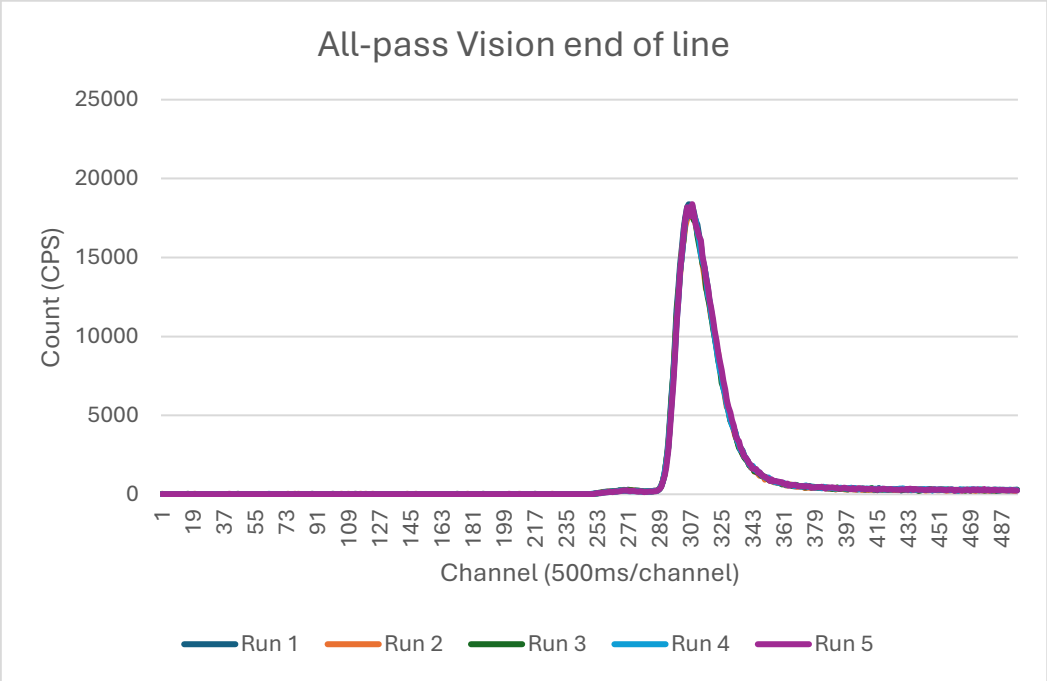

Figure 20. Vision all-pass end of line.

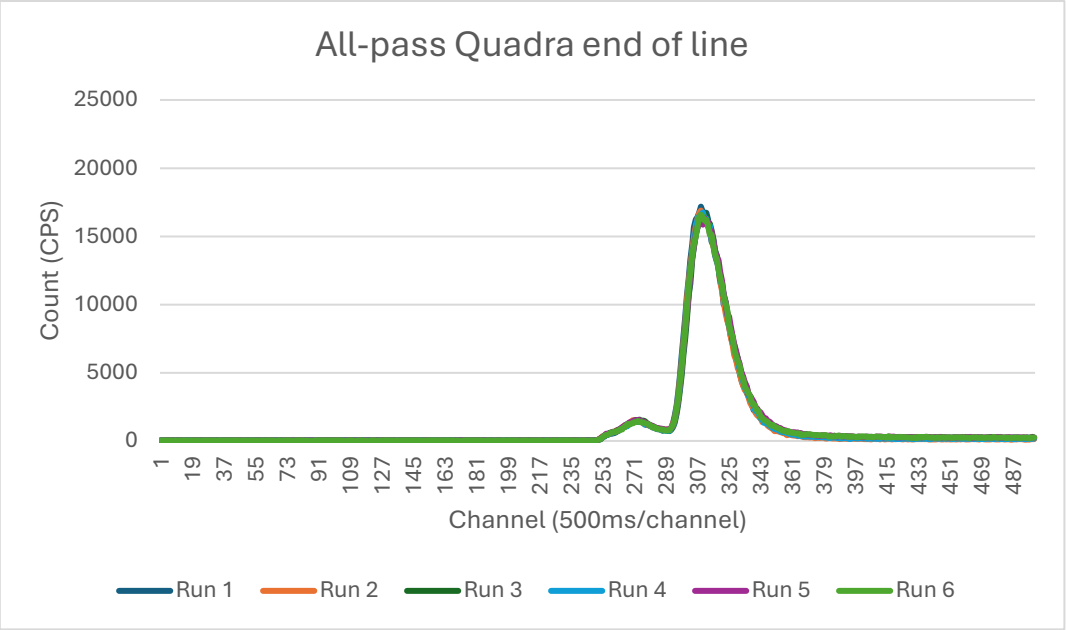

Figure 21. Quadra all-pass end of line.

Figures 20 and 21 demonstrate an all-pass bolus curve recorded by their respective end of line detectors. The radiotracer bolus reaches the detector around the channel 289 from which the steep incline of the peak begins from. After the bolus has passed the end of line detector, and has been injected into the vial, the reading returns to base level around channel 361. The detector also records a small reading between channels 253 and 289, to which the reason is unknown.

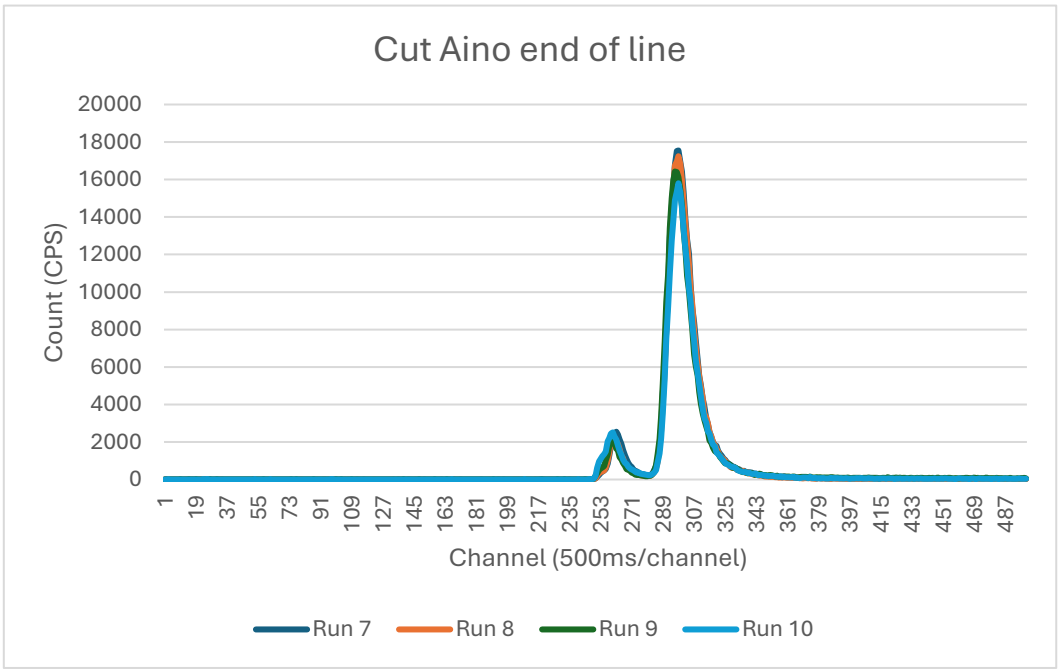

Figure 22. Aino cut end of line.

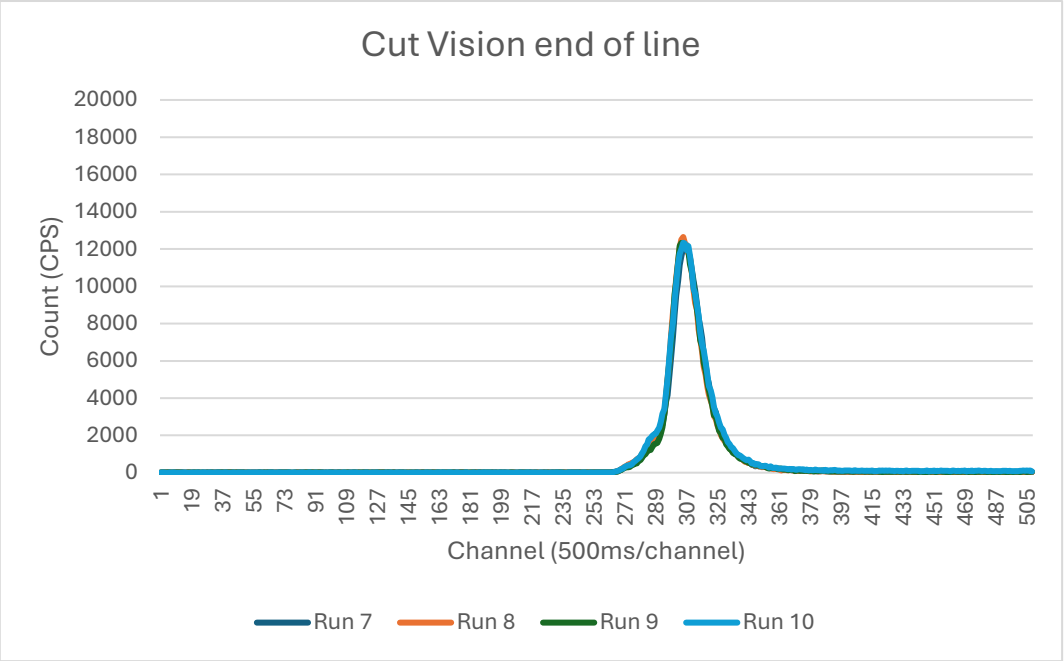

Figure 23. Vision cut end of line.

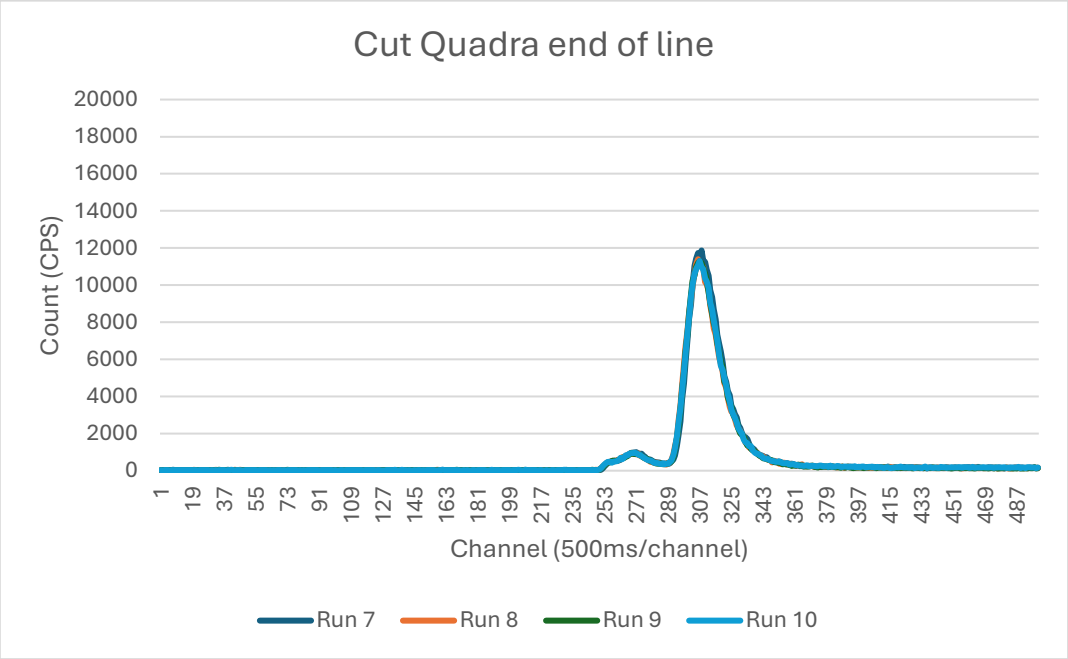

Figure 24. Quadra cut end of line.

Figures 22-24 demonstrate a cut bolus curve series from all three systems recorded by their respective end of line detectors. The radiotracer bolus reaches the detector around channel 280 (varies within detectors slightly) from which the steep incline of the peak begins from. After the bolus has passed the end of line detector, and has been injected into the vial, the reading returns to base level around channel 361.

5.3 Waste detector activity curves

Below is presented the waste line detector (located inside the measurement chamber) activity curves for all three systems in six all-pass runs (run 1-6) and four cut runs (run 7-10). It is notable that the peristatic pump used for Aino all-pass runs 1-5 had some unknown issue relating to too small flow values. The data from Vision run number 6 was lost due to circumstances not related to the monitoring add-on. It should be disclosed that peaks in the waste line after channel 490 are not relevant data when it comes to this detector. As the protocol ends around channel 490 and after that the system flushes the contents of the cartridge to the waste line causing a peak in the activity. Based on this only the first peak appearing in the waste detector line is relevant data.

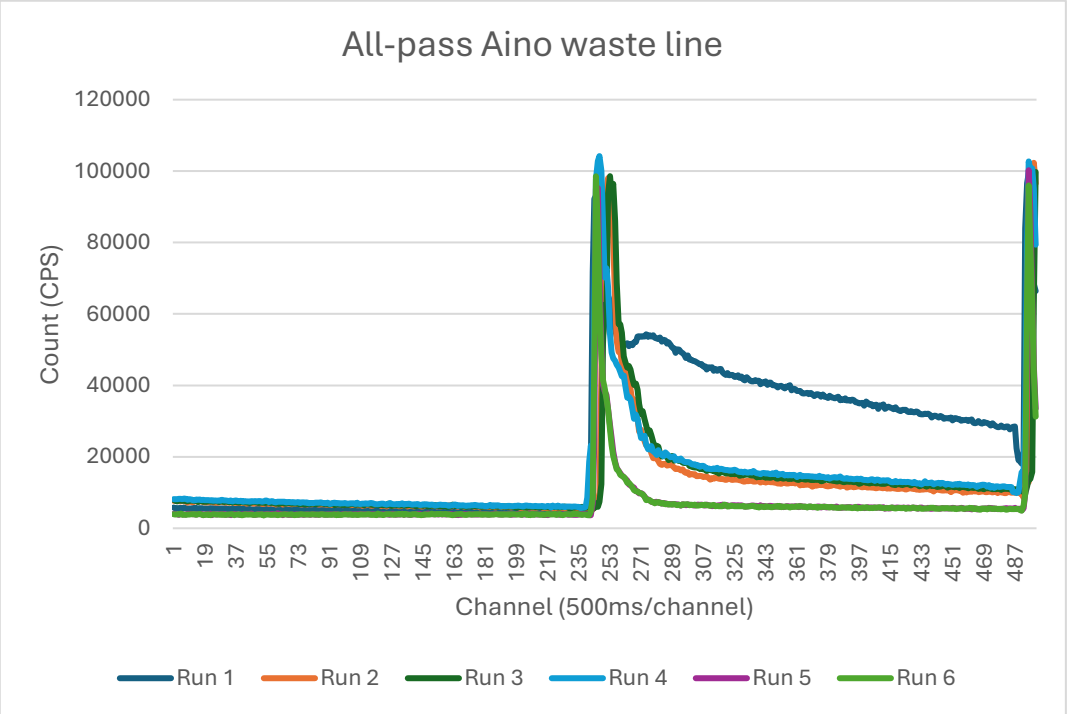

Figure 25. Aino all-pass waste line.

Figure 25 demonstrates an all-pass bolus curve series recorded by Aino waste detector. After the infusion the activity detected by the waste detector rises rapidly as the system excretes the excess activity from the chamber to the waste line. Abnormality in Run 1 should be noted, as the activity does not decrease in unison with the other runs.

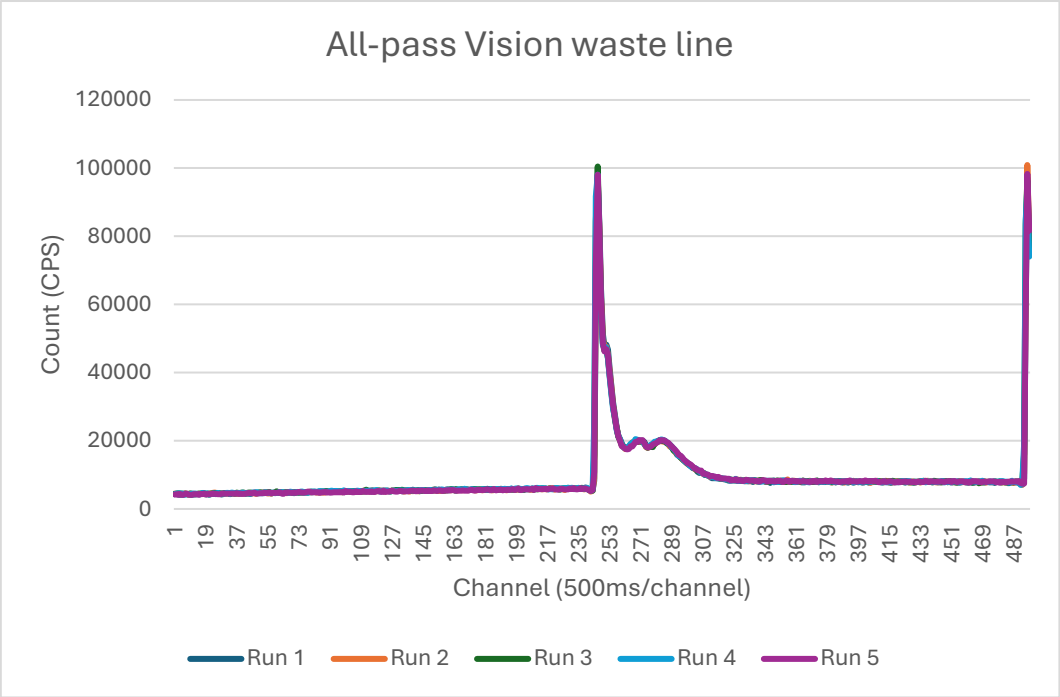

Figure 26. Vision all-pass waste line.

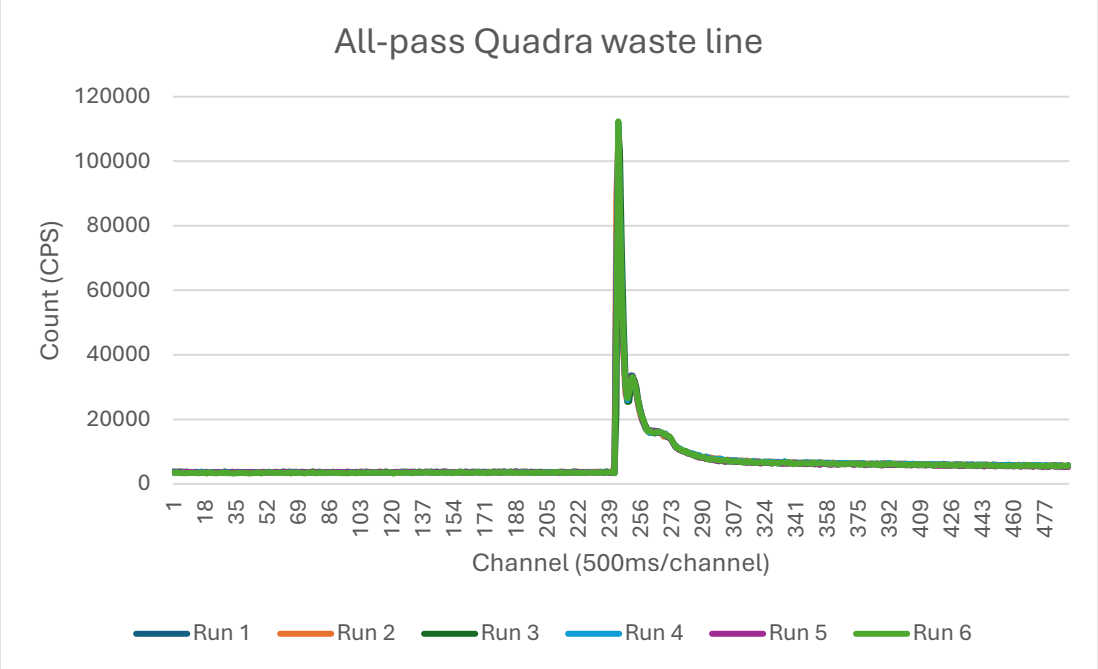

Figure 27. Quadra all-pass waste line.

Figures 26 and 27 demonstrate an all-pass bolus curve series recorded by their respective waste detectors. After the infusion the activity detected by the waste detector rises rapidly as the system excretes the excess activity from the chamber to the waste line. This is seen as a sharp incline around channel 245 (Varies within detectors slightly). After receiving the excess bolus, the waste

detector returns closer to the baseline (around channel 300) but does not descend to the exact level it was prior to the infusion due to the trace activity being introduced to the waste detector.

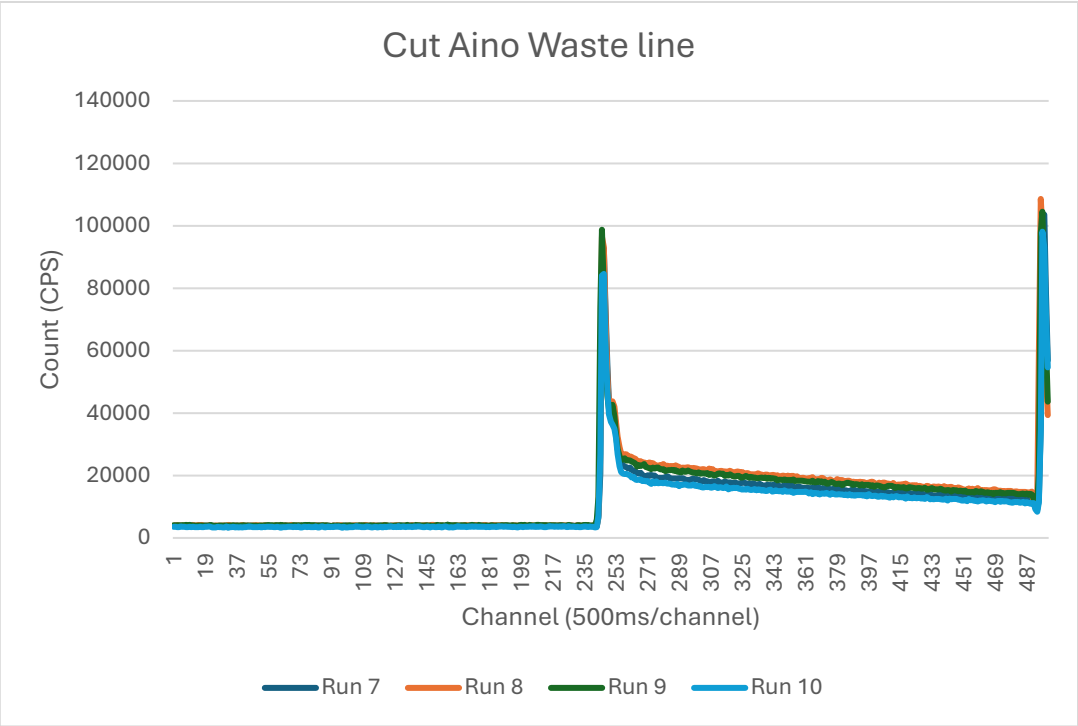

Figure 28. Aino cut waste line.

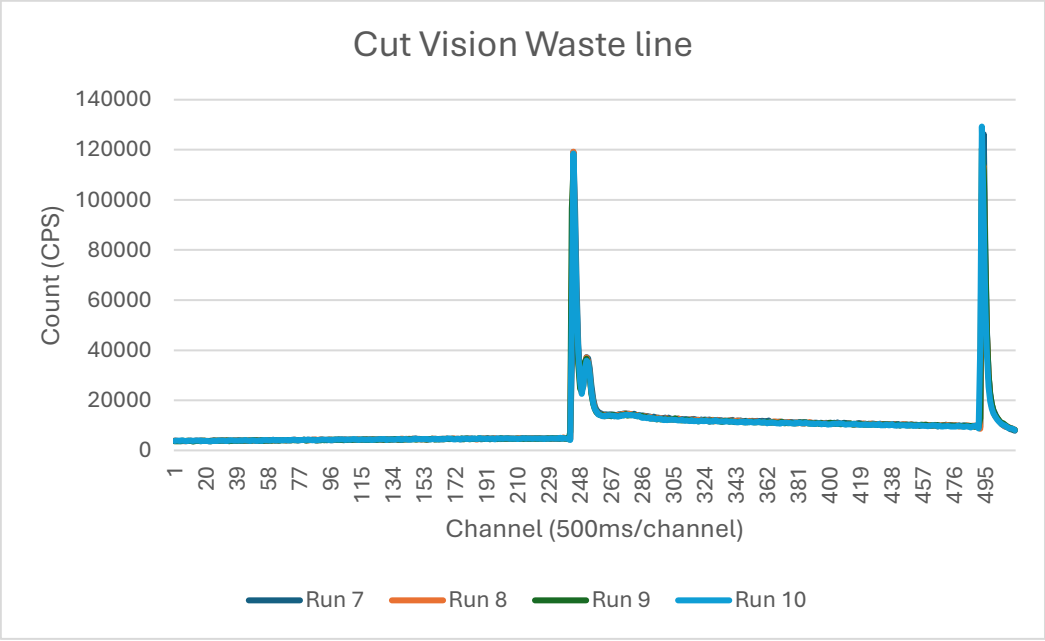

Figure 29. Vision cut waste line.

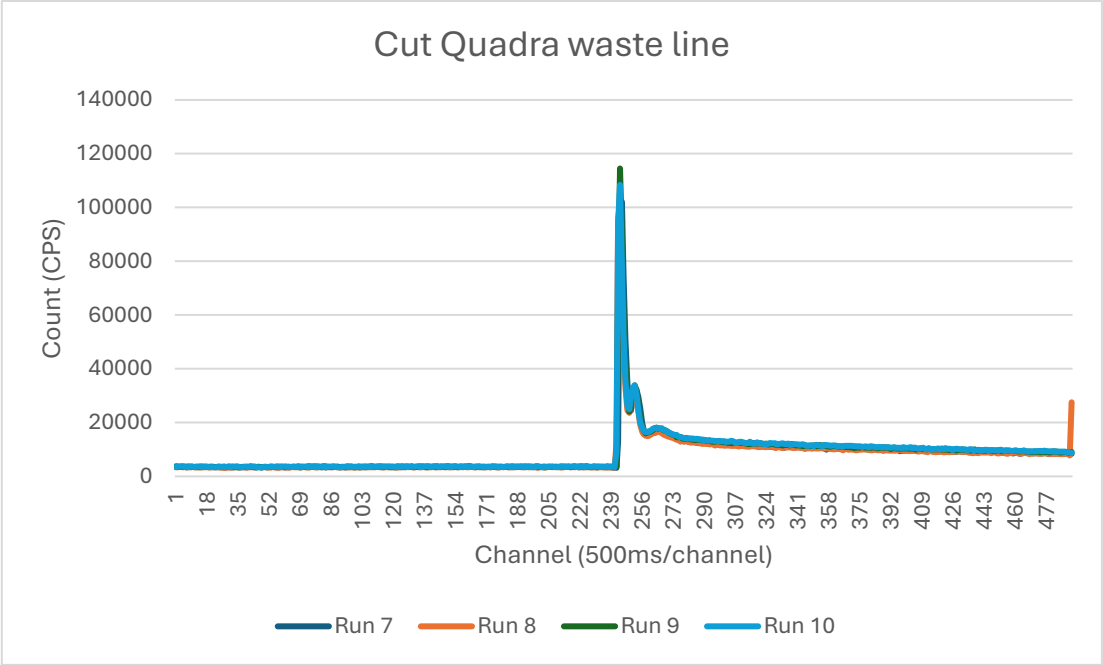

Figure 30. Quadra cut waste line.

Figures 28-30 demonstrate a cut bolus curve series from all three systems recorded by their respective waste line detectors. After the infusion the activity detected by the waste detector rises rapidly as the system excretes the excess activity from the chamber to the waste line. This is seen as a sharp incline around channel 245 (varies within detectors slightly). After receiving the excess bolus, the waste detector returns closer to the baseline (around channel 300) but does not descend to the exact level it was prior to the infusion due to the trace activity being introduced to the waste detector. The second peak seen in Figures 28 and 29 marks the end of procedure, when the cartridge flow is directed to the waste detector to flush out remaining activity. This peak is not to be included in the analysis, as it is happening outside the infusion procedure.

5.4 Incoming gas line pressure

Below is presented the gas pressure values (located in the incoming gas line of the generator) for all three systems in six all-pass runs (run 1-6) and four cut runs (run 7-10). The data from Vision run number 6 was lost due to circumstances not related to the monitoring add-on. The Tables presented below illustrate the pressure level of the gas line directed from the cyclotron to the generator. Y-axis represents the pressure in millibar scale, and X-axis represents the channel. It should be noted that for the gas pressure comparison the Y-axis is intentionally not fixed to the same value range for all measurements to emphasise the apparent gas pressure differences occurring within the systems.

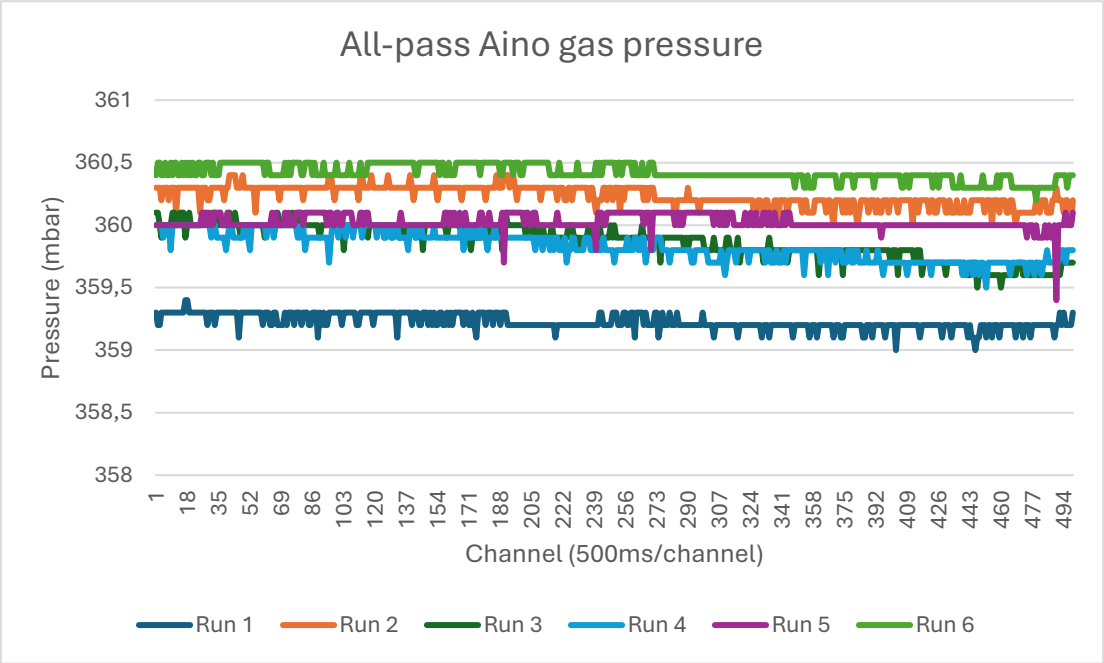

Figure 31. Aino all-pass gas pressure.

Figure 31 depicts an incoming gas pressure measurement series for all-pass runs from Aino. The gas pressure remains practically constant, which is not the expected result from this measurement series.

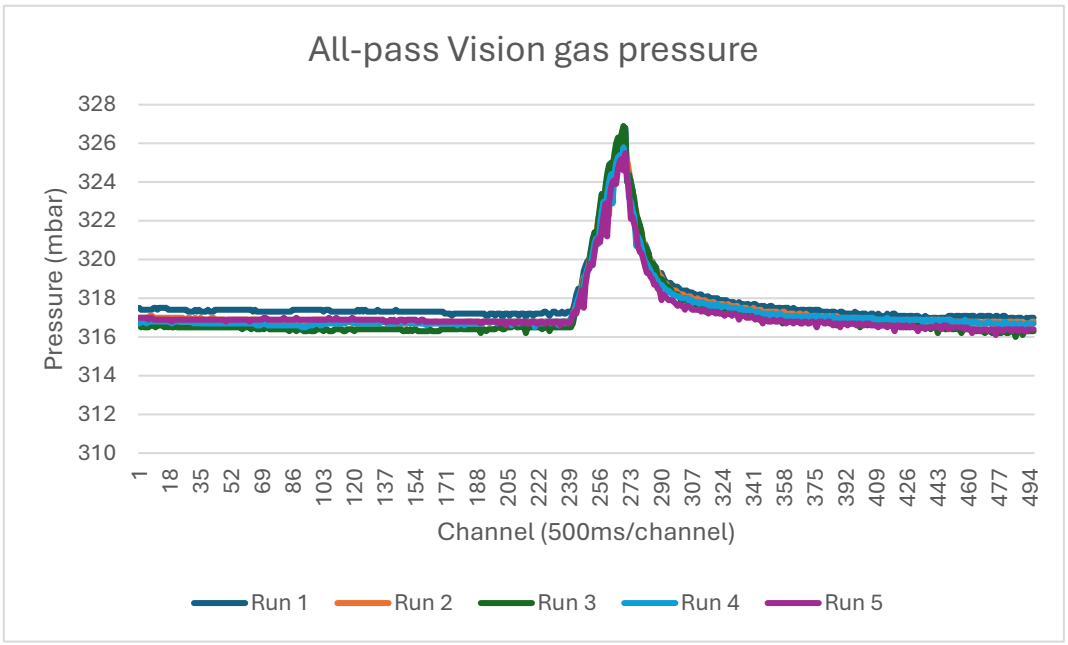

Figure 32. Vision all-pass gas pressure.

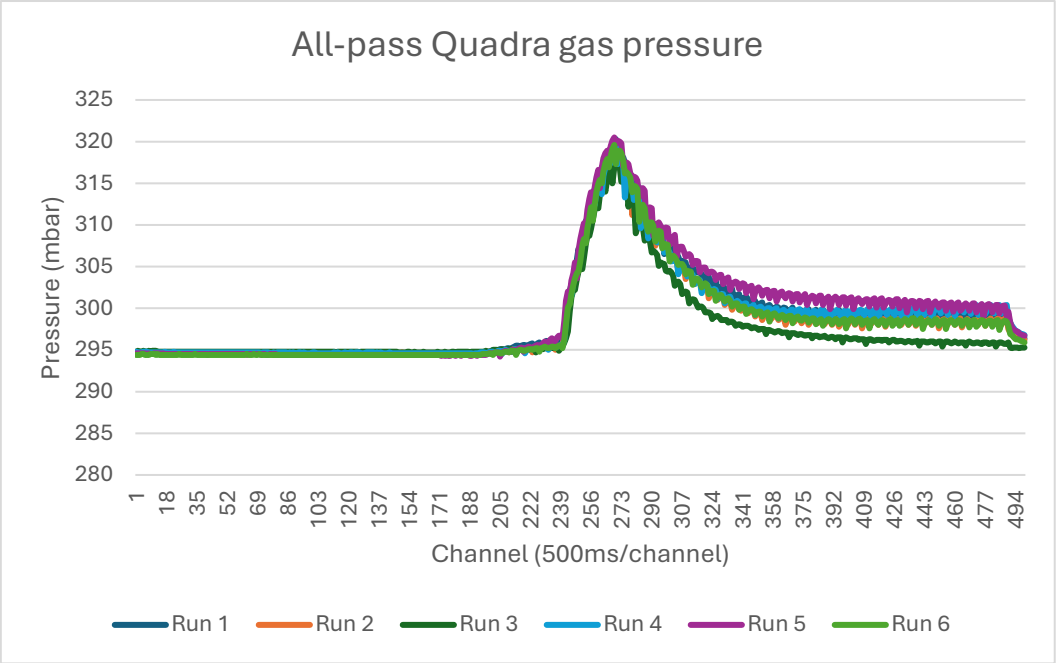

Figure 33. Quadra all-pass gas pressure.

Figures 32 and 33 demonstrate an all-pass incoming gas pressure measurement series from Vision and Quadra recorded by their respective gas pressure monitors. From these Figures, the gas pressure can be seen increasing during the infusion (starting from channel 240) and then gradually return to base level after infusion.

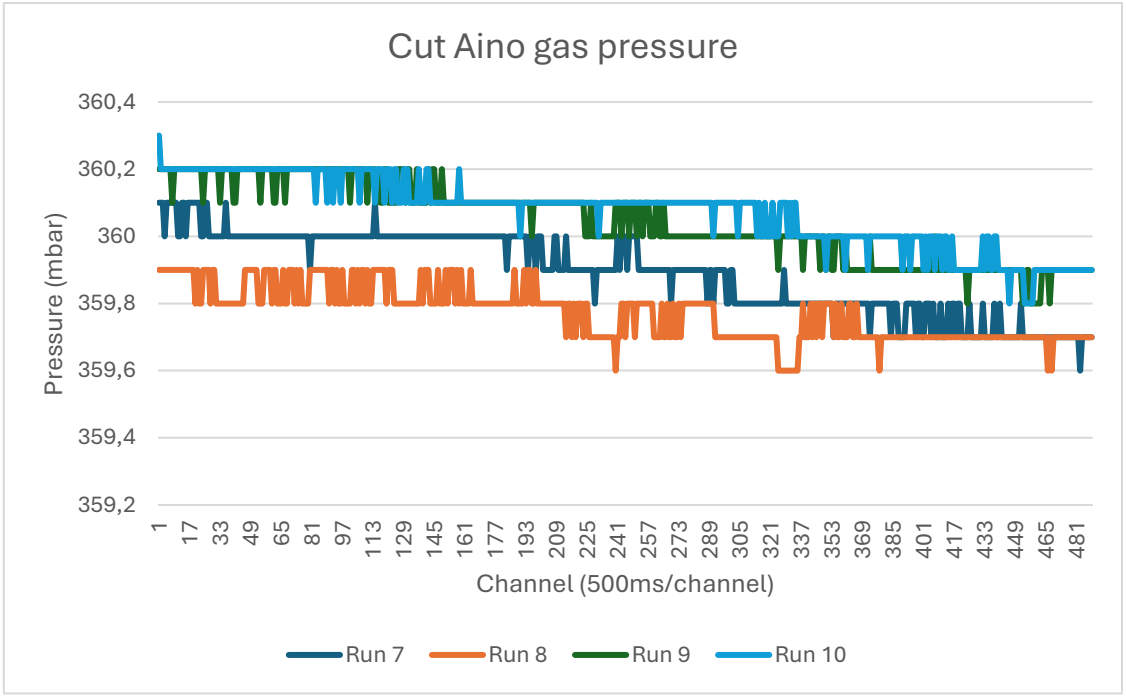

Figure 33. Aino cut gas pressure.

Figure 33 depicts an incoming gas pressure measurement series for cut runs from Aino. The gas pressure remains practically constant, which is not the expected result from this measurement series.

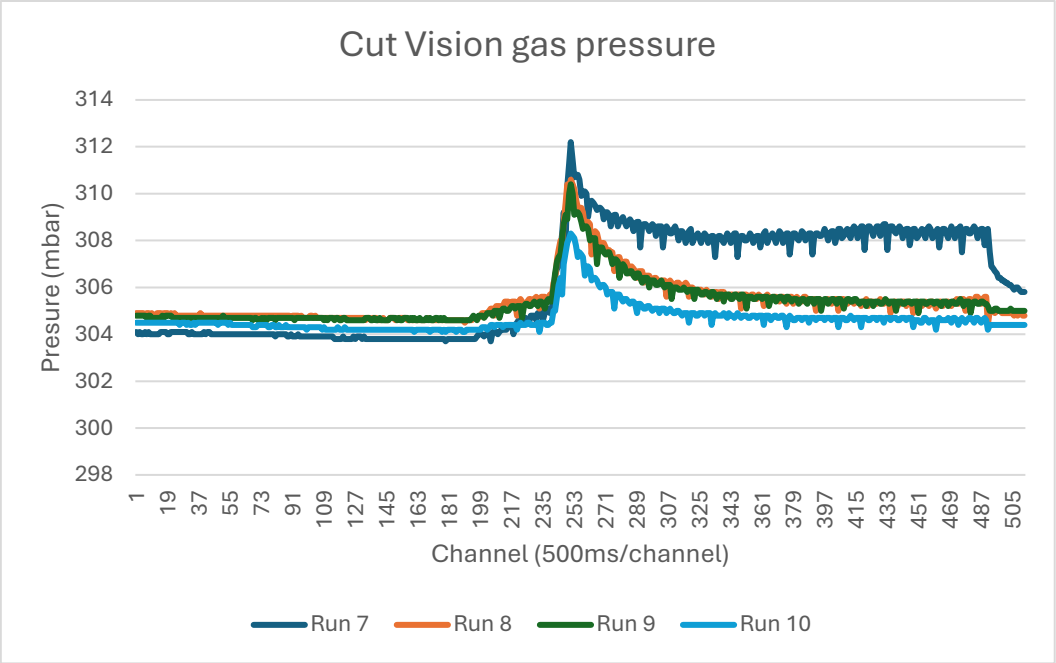

Figure 34. Vision cut gas pressure.

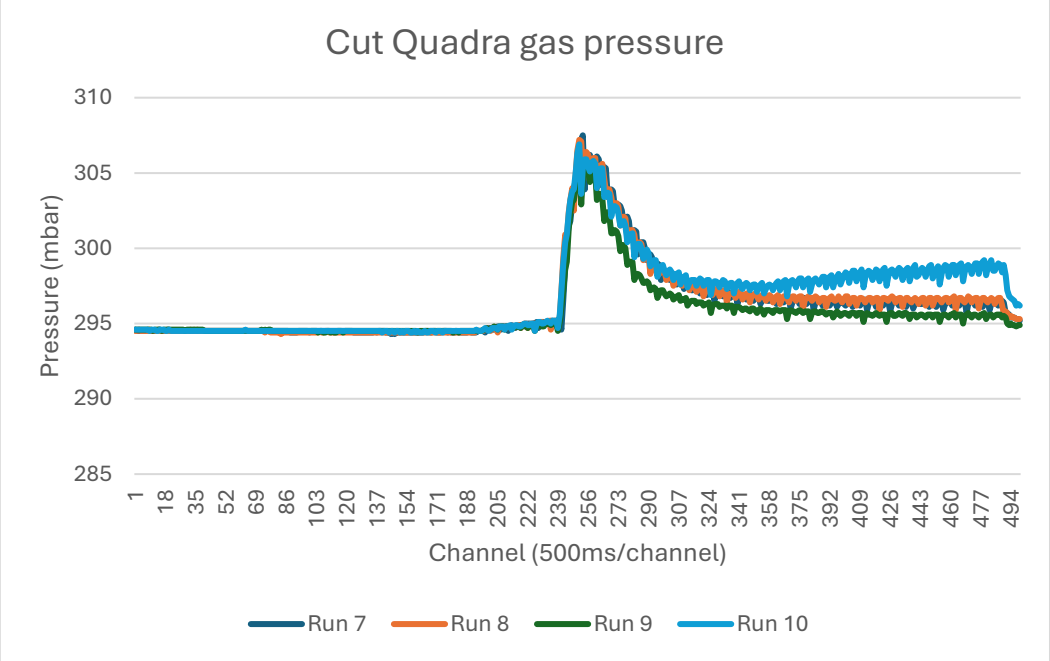

Figure 35. Quadra cut gas pressure.

Figures 34 and 35 demonstrate an all-pass incoming gas pressure measurement series from Vision and Quadra recorded by their respective gas pressure monitors. From these Figures, the gas pressure can be seen increasing during the infusion (starting from channel 240) and then gradually return to

base level after infusion. The base level of the pressure varies slightly between these Figures, and the decline rate seems to fluctuate slightly as well.

5.5 Liquid pressure in the patient line

Below is presented the liquid pressure values (sensor located in the patient line between the peristatic pump and infusion point) for all three systems in six all-pass runs (run 1-6) and four cut runs (run 7-10). The data from Vision run number 6 was lost due to circumstances not related to the monitoring add-on. The Tables presented below illustrate the pressure level of the patient line after the peristatic pump. Y-axis represents the pressure in millibar scale, and X-axis represents the channel. It is notable that the peristatic pump used for Aino all-pass runs 1-5 had some unknown issues relating to too small flow values which resulted in unstructured data regarding the runs 1-5 as the pressure reading alternated between 0 and the assumed baseline. This data is still presented to demonstrate the issues that can be expected with dysfunctional peristatic pump. However, only the run 6 is regarded as relevant data for Aino all pass runs in the liquid pressure measurements.

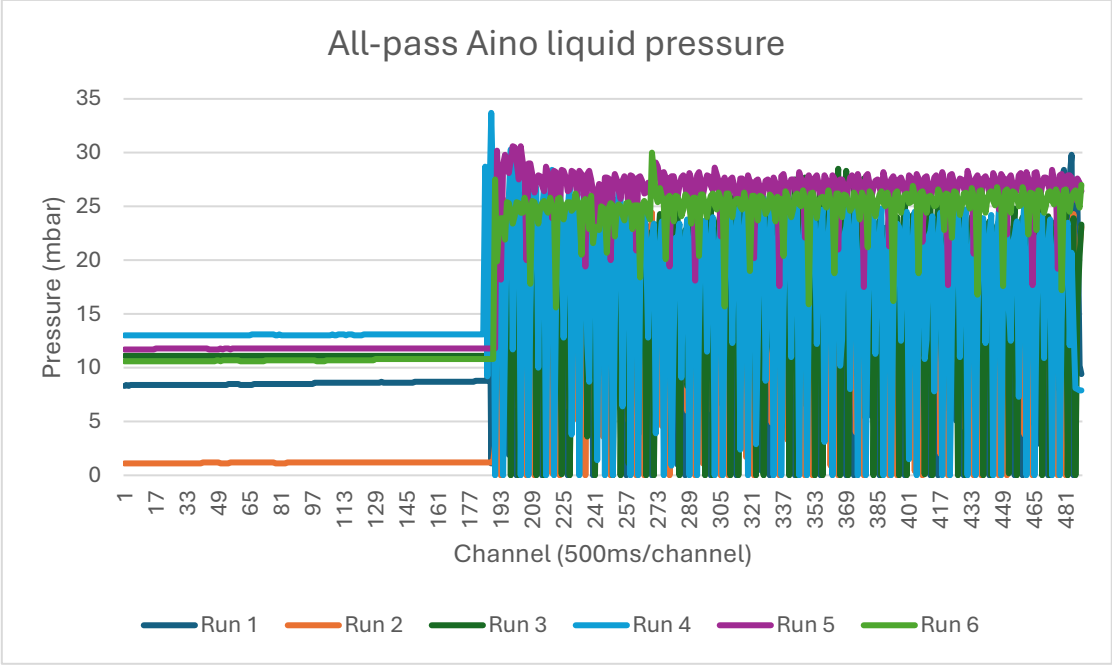

Figure 36. Aino all-pass liquid pressure.

Figure 36 depicts an incoming liquid pressure measurement series for all-pass runs from Aino. The fluctuation in liquid pressure due to the peristatic pump issues is prominent in runs 1-5. Run six is an expected result, where the liquid pressure increases from the baseline at the start of the infusion and remains in the elevated state throughout the procedure (until channel 490).

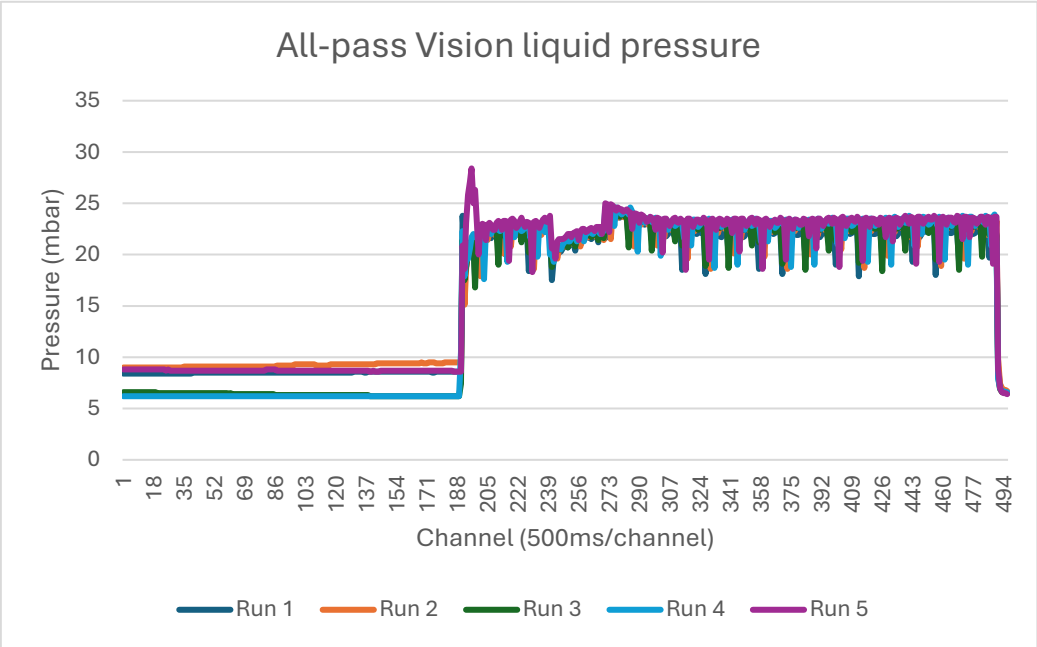

Figure 37. Vision all-pass liquid pressure.

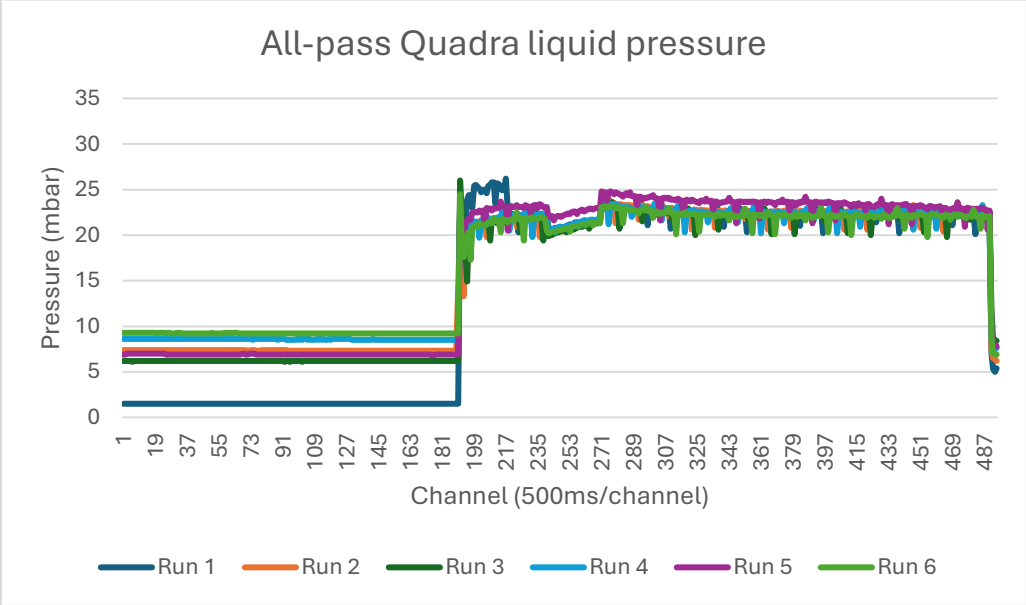

Figure 38. Quadra all-pass liquid pressure.

Figures 37 and 38 demonstrate an all-pass incoming liquid pressure measurement series from Vision and Quadra recorded by their respective liquid pressure monitors. From these Figures, the liquid pressure can be seen increasing during the infusion (starting from channel 240) and then returning to base level after the procedure is completed (channel 490).

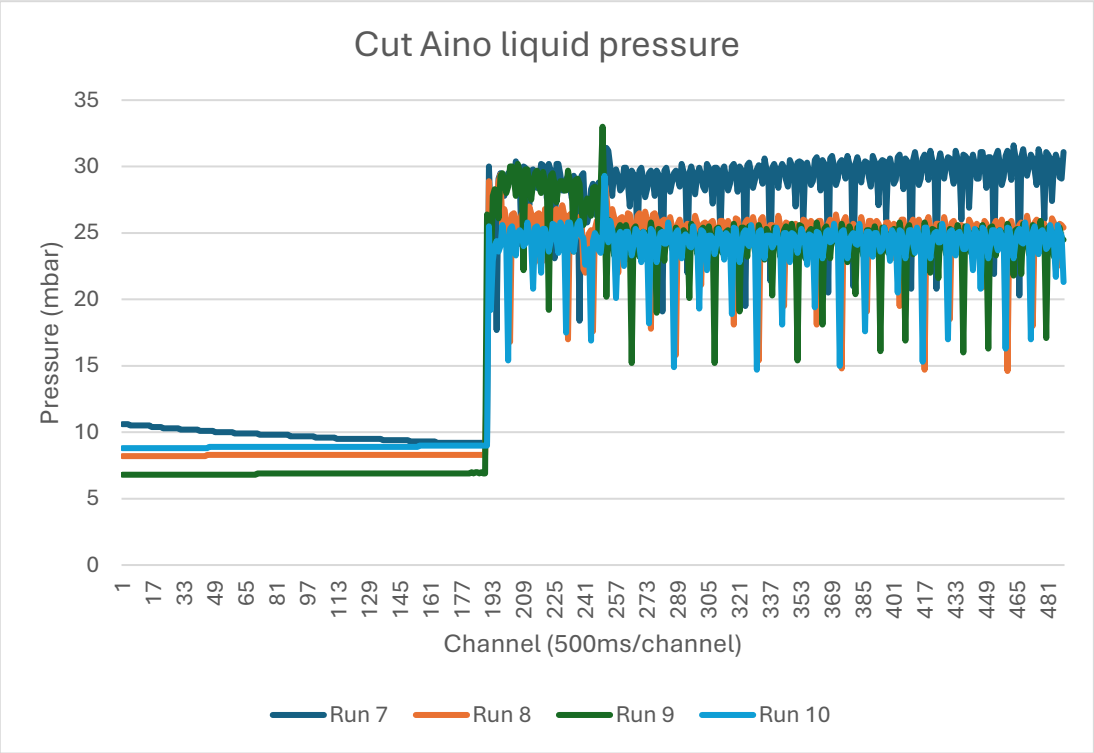

Figure 39. Aino cut liquid pressure.

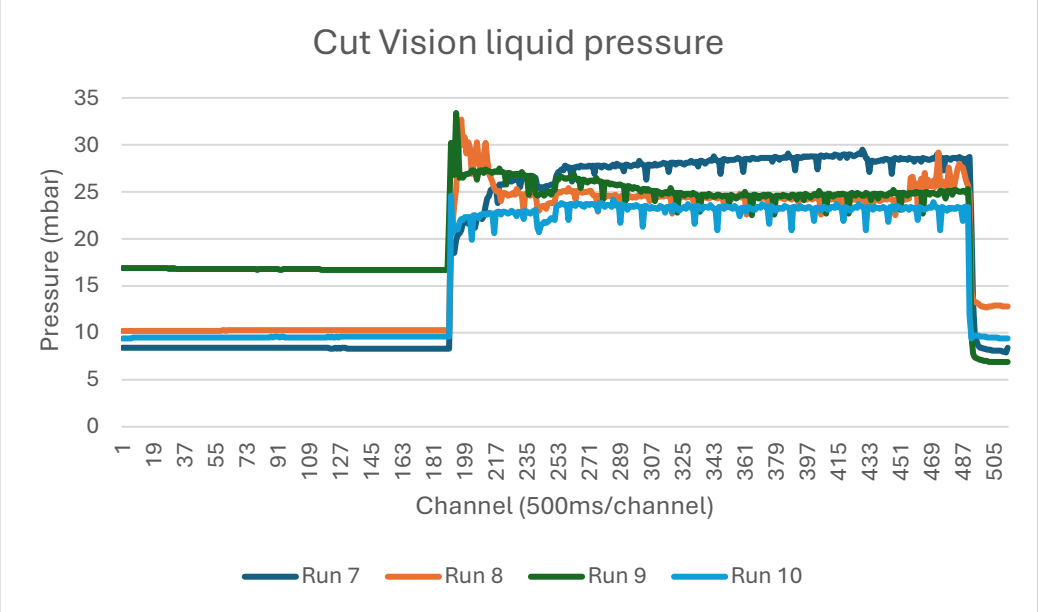

Figure 40. Vision cut liquid pressure.

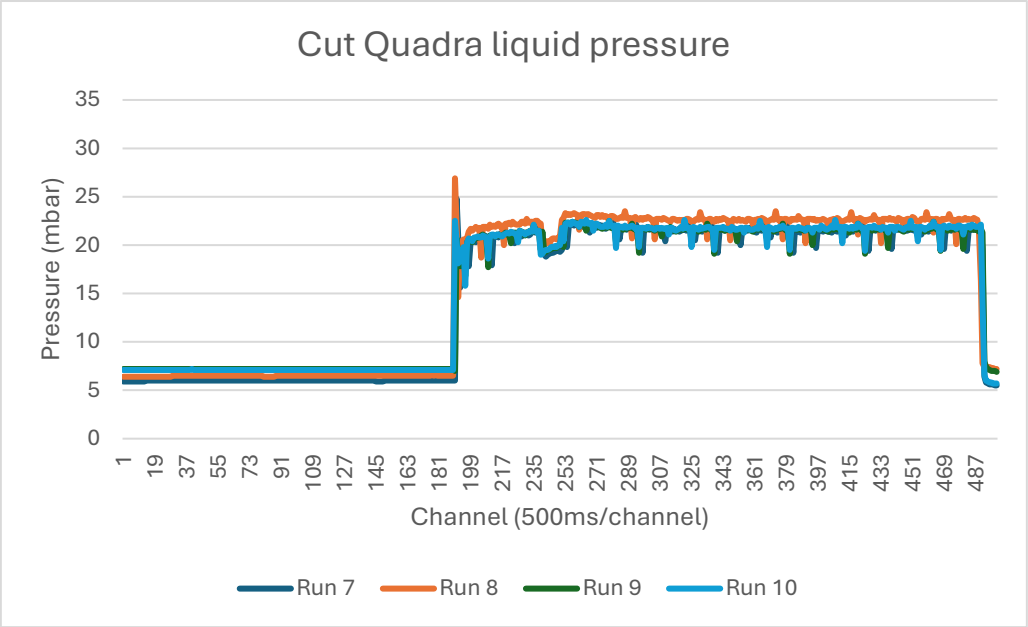

Figure 41. Quadra cut liquid pressure.

Figures 39-41 demonstrate a cut incoming liquid pressure measurement series from all three systems recorded by their respective liquid pressure monitors. From these Figures, the liquid pressure can be seen increasing during the infusion (starting from channel 240) and then returning to base level after the procedure is completed (channel 490). The base level of the liquid pressure seems to vary slightly within these measurements, but the level of increase seems to be very consistent, as are the pressure changes within the systems around channel 253.

5.6 Activity curve spectrum analysis

Below is presented the conducted spectrum analysis for the activity curves recorded with the monitoring add-on across all three systems. This is presented to demonstrate curve characteristics such as width regarding FWHM and area regarding AUC. The Tables also include a column for "patient max channel" which represents the location of the bolus peak in each system as a channel value. All-pass and cut protocols are separated into their own designated Tables (Tables 2 and 3) and AUC values are recorded and further processed (regarding average and standard deviation) in their own designated Table (Table 4) in order to better demonstrate the possible differences. It should be noted that the results from Aino all-pass runs are not included in this AUC analysis Table 4 due to a known error with the peristatic pump that resulted in unusable data.

Table 2. Activity curve analysis for all-pass

System	Run #	Patient FWHM (Channel)	Patient max channel	Patient AUC (Count)	EoL FWHM (Channel)	EoL AUC (Count)	Waste FHWM (Channel)	Waste AUC (Count)
Aino	Run 1	5	256	474685	21	787820	60	10050315
	Run 2	10	268	504859	31	761129	11	4144015
	Run 3	14	272	545478	35	797678	12	4518152
	Run 4	13	264	561152	35	837108	10	4812229
	Run 5	6	255	292689	20	493666	4	2118754
	Run 6	6	254	297809	20	530022	3	2102905
Vision	Run 1	6	253	287071	25	553537	5	3015217
	Run 2	6	253	279544	26	536888	5	3028950
	Run 3	7	253	282905	25	540367	4	3051859
	Run 4	6	253	289391	24	544011	4	3068866
	Run 5	6	253	285352	24	549977	4	3042133
Quadra	Run 1	8	254	324894	25	542647	4	2320341
	Run 2	7	254	324309	25	518764	4	2345858
	Run 3	8	254	319204	25	540719	3	2269890
	Run 4	8	254	320446	25	526647	4	2336886
	Run 5	8	254	316841	27	551665	4	2254195
	Run 6	8	254	315614	25	543147	3	3087707

Table 3. Activity curve analysis for cut

System	Run #	Patient FWHM (Channel)	Patient max channel	Patient AUC (Count)	EoL FWHM (Channel)	EoL AUC (Count)	Waste FHWM (Channel)	Waste AUC (count)
Aino	Run 7	5	255	182881	15	350617	4	4373628
	Run 8	4	254	173892	15	335522	4	5115608
	Run 9	4	254	177608	15	330091	4	4868473
	Run 10	4	254	172872	15	318926	4	318926
Vision	Run 7	5	254	170698	20	307972	3	3341314
	Run 8	5	253	168656	19	308858	3	3318871
	Run 9	5	253	171157	19	305443	3	3299655
	Run 10	5	253	165071	21	329694	3	3242204
Quadra	Run 7	4	254	178692	20	328246	3	3087707
	Run 8	4	253	173206	19	316987	3	3041453
	Run 9	4	253	175651	19	316989	4	3286596
	Run 10	4	253	173899	21	321064	3	3343197

Table 4. AUC analysis table

Patient AUC comparison								
System	All-pass AUC Min (Count)	All-pass AUC Max (Count)	All-pass AUC Average (Count)	All pass AUC Standard deviation	Cut AUC Min (Count)	Cut AUC Max (Count)	Cut AUC Average (Count)	Cut AUC standard deviation
Aino	-	-	-	-	172872	182881	176813	4528
Vision	279544	289391	284852	3799	165071	171157	168895	2771
Quadra	315614	324894	320218	3802	173206	178692	175362	2446
End of line AUC comparison								
Aino	-	-	-	-	318926	350617	333789	13175
Vision	536888	553537	544956	6817	305443	329694	312991	11228
Quadra	518764	551665	537264	12148	316987	328246	320821	5309
Waste AUC comparison								
Aino	-	-	-	-	318926	5115608	3669158	2254691
Vision	3015217	3068866	3041405	20644	3242204	3341314	3300511	42435
Quadra	2254195	3087707	2435812	321463	3041453	3343197	3189738	147569

Below is presented spectrum analysis Tables (Table 5 all- pass and Table 6 cut) from the RWG patient detector values obtained from each of the systems. It is important to note that the RWG system has an unknown correction factor when processing the detected counts (which is apparent when comparing the AUC values of all-pass and cut runs), and the AUC value therefore is not directly comparable to the value produced by the monitoring add-on. The RWG patient AUC can still be indirectly used to represent variability within the systems. The significant values from the RWG detector analysis chart are the "patient max channel" which demonstrates the timing of the systems against the monitoring add-on and the "patient FWHM" which demonstrates the bolus curve shape against the monitoring add-on. The RWG patient detector Tables are also separated according to the used protocol, all-pass and cut.

Table 5. RWG Activity curve analysis for all-pass

System	Run #	Patient FWHM (Channel)	Patient AUC (Count)	Patient max channel
Aino	Run 1	4	4980	258
	Run 2	11	6952	269
	Run 3	14	5662	270
	Run 4	13	4222	268
	Run 5	6	3871	253
	Run 6	6	4197	253
Vision	Run 1	6	4734	254
	Run 2	7	4578	254
	Run 3	7	4688	253
	Run 4	6	4730	254
	Run 5	7	4614	254
	Run 6	7	4671	253
Quadra	Run 1	7	3954	253
	Run 2	7	3996	253
	Run 3	7	3891	254
	Run 4	7	3912	254
	Run 5	7	3896	253
	Run 6	7	3942	253

Table 6. RWG Activity curve analysis for cut

System	Run #	Patient FWHM (Channel)	Patient AUC (Count)	Patient max channel
Aino	Run 7	5	59198938	253
	Run 8	5	55410292	253
	Run 9	4	56298856	253
	Run 10	5	56445704	252
Vision	Run 7	5	60434712	254
	Run 8	5	61001928	253
	Run 9	5	62010000	253
	Run 10	5	58613256	254
Quadra	Run 7	5	56845872	253
	Run 8	4	54710312	253
	Run 9	4	55041692	253
	Run 10	4	54667180	254

6 Discussion

This thesis aimed to successfully install the monitoring add-on to three different radiowater generator units in Turku PET Centre and analyse the data that was acquired from each of the units. The target was to analyse each of the units as individual systems and also compare the produced results among all of the units regarding repeatability and reproducibility. One of the research questions was also to compare the data produced by the monitoring add-on against the data produced by the RWG units current UI. This chapter contains the evaluation of these questions in designated sub-chapters.

In this thesis the monitoring add-on was installed to three different RWG systems Aino, Vision, and Quadra. Results responding to the time activity curves for each of the three detectors, liquid pressure, gas pressure and bolus curve characteristics were acquired. From each system six all-pass runs (Vision only 5) and 4 cut runs were recorded. As noted, the first 5 all-pass runs with Aino were compromised due to an issue in the peristatic pump and are only presented to demonstrate the potential error cases due to instrumentation. Therefore, Aino runs 1-5 are excluded from this analysis from this point on (exception 6.4 Study Limitations).

6.1 Individual system evaluation

Regarding the repeatability and reproducibility of the time activity curves acquired from each unit, the results are reassuring. All three detectors (patient, waste and end of line) seem to produce nearly identical results in both all-pass and cut runs, and only minor differences in bolus shape can be detected within units (Tables 2-4). The bolus timing is also very consistent within units, as the difference in the peak value detection (patient max channel) is only one channel (500 milliseconds) at its highest which is presented in Tables 2 and 3.

The recorded gas pressure values were similar within one unit but when compared to each other the values produced by different units vary significantly (discussed in 6.2). There is, however, some variation in these values, for example the Vision cut gas pressure (Figure 34) demonstrates the gas pressure sensor readings not lining up perfectly with different runs. The variation is not very significant, being about 5 millibars apart from one another, but this is still a noteworthy observation. This could be related to some pressure build-up or temporal blockage within the system.

Liquid pressure within units was also relatively similar, especially within Quadra and Vision, but Aino liquid pressure in cut runs seemed to vary a bit more according to Figure 39. Similarly to the

gas pressure, the variance is not very large, being only about 5 millibars, but it is still abnormal to see any variability in the liquid pressure, as the conducted runs are identical and there should not be major pressure changes in the patient line. A noteworthy phenomenon is also the variability in the base level of the liquid pressure (channel 0-240). In Quadra all-pass (Figure 38), the base level fluctuation is only seen in the first measurement, and this is most likely due to the line not being pressurised in beginning of the measurements. But for example, the base level fluctuation in Vision cut (Figure 40) is very unlikely to have the same explanation and the reason for the base level change remains unknown.

The results presented in time activity spectrum analysis seem to be very consistent within units. As stated before, the curve timing practically does not deviate at all within units. The bolus curve width (represented by FWHM) is also very repetitive in all the detectors. Variability regarding the AUC is demonstrated in Table 4. The variability represented by standard deviation seems to be very minor within each unit, except for the Aino waste detector AUC values in Cut runs. The standard deviation within this unit is very significant as is the difference between the min and max AUC values. Upon further investigation of Table 3, it can be seen that Aino run number 10 has significantly lower AUC value in the waste detector. As the area under the curve is smaller, one would expect that the time activity curve for said detector would be much lower than its counterparts. As we examine Table 2, it is indeed visible that the waste detector activity curve of run number 10 is lower than its counterparts. From visual inspection of the spectra (Figure 28), it does not necessarily seem to be very alarming, but from the AUC values we can see that there is a significant difference to the other runs.

6.2 Comparison of different systems

Differences among these three systems are discussed in this chapter. Time activity curves within these different systems seem to be rather similar, with minor differences mostly in curve height. The timing of the curves is very similar as we examine the patient max channel value presented in Tables 2 and 3. In other systems, there appears to be a slight “bump” in the end of line bolus curve before the actual bolus is recorded, for example when we compare Figures 22, 23 and 24. Most likely this is due to the sensitive nature of the detectors, and the shielding of the add-on module or the patient line varies slightly as the module is installed to a different RWG unit. However, the bump can be dismissed as it is very minimal in comparison to the actual bolus. This is brought to attention only to emphasise the necessity of proper sheltering of the detectors.

As noted in chapter 6.1 the differences between the recorded gas pressure values are very prominent. Units Vision and Quadra seem to follow each other somewhat regarding the gas pressure, but Aino is not producing similar results to the other units regarding the values or the shape of the gas pressure change. In Vision and Quadra, the gas pressure seems to spike up upon the start of the infusion, and then gradually decline back to the base level. In Aino however, the pressure level is more or less stagnant throughout the whole procedure. It could be that the pressure does not alternate as the base level is already very high, and the system is simply operating at maximum pressure constantly. This is certainly an interesting phenomenon for which there is no explanation for as of now. A suggested reason for this pressure difference could be related to the cyclotron-RWG gas line connection, or some variability within the three systems. However, the gas pressure is not something that the monitoring add-on has access to regulate or adjust, and therefore it can only be observed.

Liquid pressure seems to be very consistent within the different units, besides the base level changes and slight abnormalities in Aino described in previous chapter. The curve characteristics also seem to be very similar within different units. Arguably, the timing is the most important parameter in this comparison and as Tables 2 and 3 demonstrate, the timing difference among these units is 2 channels (1 second) at the highest. This is seen as a very positive characteristic when it comes to interchangeability of the add-on within different RWG units.

6.3 Comparison against the current system

When comparing the results produced by the monitoring add-on to the results produced by the RWG user interface, it is vital to note again that the AUC values of these systems are not interchangeable, as the RWG logic employs an unknown correction factor to the count values. RWG AUC is only presented in the results to further demonstrate the similarity of these runs. Therefore, the major focus is on the timing of the patient detector peak timing, peak width and variance in those two parameters.

As we examine the patient detector max value from Tables 5 and 6 and compare those to the ones in Tables 2 and 3, it is apparent that the timing of the monitoring add-on practically has no difference to the RWG. This is a good discovery regarding the research question "*Is the data produced by the monitoring add-on comparable to the data produced by RWG system?".* The patient detector similarity can also be further emphasised by comparing the FWHM values in Tables 2 and 3 versus Tables 5 and 6. Interestingly, the patient detector bolus peak seems to be slightly wider in all-pass runs than in cut runs. This could be due to the fact that all-pass runs have a longer duration in the

infusion, and the activity “piling” could cause this peak to become wider. The peak width change is, however, seen both in RWG and the monitoring add-on and therefore supports the similarity of the produced data.

6.4 Study limitations

The limitations of this study were mainly related to instrumentation. As mentioned previously multiple times, the peristatic pump for Aino runs 1-5 was dysfunctional and that distorted the acquired data from those runs. Another aspect is the difference in incoming gas base-level values for each of the three systems used. This is something that the monitoring add-on has no control over but mapping the starting conditions for each system prior to conducting the tests could prove to be beneficial in the result examination phase. In this project three systems were used in the monitoring add-on evaluation, but Turku PET Centre has one more RWG that is designated to PET/MRI. This scanner, however, was deemed not to be suitable for this purpose of testing due to the monitoring add-on containing several metallic parts. The established magnetic field around the PET/MRI scanner makes this scanner not appropriate or safe for this purpose of testing.

Another limitation is the RWG system unknown correction factor described in chapter 6.3. The data regarding the counts is not uniform, as the RWG logic processes counts according to an unknown correction factor. Also, there has not been an in-depth component comparison between the monitoring add-on photon counting modules and the RWG photon counting component and their differences in counting efficiency. A calibration factor or other data uniformization tool would be beneficial in future comparisons. This would require in-depth embedded software knowledge, to determine the RWG correction factor and to develop a response.

At the time of performing these measurements, the calibration status or requirement of each photodetector unit was unknown. In the construction of this monitoring add-on each detector was calibrated to similar state, but detector differences are not investigated during the data acquisition phase of this thesis. Detector calibration and comparison is something that is being done with the monitoring add-on currently, but is not included in this project. Due to this calibration uncertainty, certain detectors may be of different sensitivity as their counterparts, and may or may not produce different results if the location specified detectors were to be changed to a different location. For example, patient detector to end of line.

6.4 Future prospects

Future prospects include possible installation to other RWG units than the three used in this test, Aino, Vision or Quadra. The system could be transported to other PET imaging facilities for example in KYS or HUS and evaluate their RWG systems. Phantom testing using this monitoring add-on is already planned for Turku PET Centre, and effects of backpressure to the bolus shape are to be recorded using this monitoring add-on and a backpressure phantom. This monitoring add-on in its entirety or parts of it (for example liquid pressure) could also be used in laboratory animal tests as supplementary monitoring.

The utilisation of the monitoring add on for in-vivo tests is a matter of medical device guidelines and system sterility. In this project the sterility of the system was not evaluated as it was not deemed significant for this system testing purpose. In the possible case that sterility of the system would become a timely topic, the components should be re-evaluated especially regarding the in-line nature of certain monitoring components, such as the liquid pressure sensor.

7 Conclusions

This monitoring add-on was successfully installed to three different RWG systems, and the results were deemed to be repeatable and stable. When comparing the results produced by the monitoring add-on and the current RWG control software, the results were deemed to be in unison regarding the monitored parameters (bolus timing).

8 Acknowledgements

First and foremost, I want to thank my supervisors Dr. Reetta Siekkinen, Dr. Jarmo Teuho and Prof. Riku Klén for their invaluable expertise and active guidance throughout this thesis project.

I would also like to thank the people directly involved in this thesis project: Hannu Sipilä, Henry Hsiao, Heidi Partanen and Emilia Puhakka.

Lastly, I would like to thank the Turku PET Centre grant committee for providing me with a grant for this thesis project as a part of their master's level PET imaging themed research funding.

9 References

1. Fahey F, Stabin M, Dose Optimization in Nuclear Medicine, Seminars in Nuclear Medicine, Volume 44, Issue 3, 2014, Pages 193-201, https://doi.org/10.1053/j.semnuclmed.2014.03.006.

2. Johns Hopkins medicine (n.d) - Positron Emission Tomography (PET) https://www.hopkinsmedicine.org/health/treatment-tests-and-therapies/positron-emission-tomography-pet#:~:text=Positron%20emission%20tomography%20(PET)%20is,nuclear%20medicine%20and%20biochemical%20analysis Webpage cited in 24.10.24

3. Atanda O, West J, Stables T, Johnson C, Merrifield R, Kinross J. Flow rate accuracy of infusion devices within healthcare settings: a systematic review. Ther Adv Drug Saf. 2023 Jul 21; 14:20420986231188602. https://doi.org/10.1177/20420986231188602

4. Techniques in the Behavioural and Neural Sciences, Intravenous Drug Administration, Editor(s): V. Claassen, Elsevier, Volume 12, 1994, Pages 5-22, ISSN 0921-0709, ISBN 9780444818713, https://doi.org/10.1016/B978-0-444-81871-3.50007-2

5. Siikonen M. Measurement uncertainty of the bolus curves produced by a radiowater generator. Jul 24, Pro Gradu, University of Turku Department of Physics and Astronomy https://urn.fi/URN:NBN:fi-fe2024080263360

6. Siekkinen R, Partanen H, Kukola L, Tolvanen T, Fenwick A, Smith N. A.S.; Teräs M, Saraste A, Teuho J. Preliminary protocol for measuring the reproducibility and accuracy of flow values on digital PET/CT systems in [15O]H2O myocardial perfusion imaging using a flow phantom. Springer Nature, EJNMMI Physics (1/11) 2024. https://doi.org/10.1186/s40658-024-00654-y

7. National Research Council (US) and Institute of Medicine (US) Committee on the Mathematics and Physics of Emerging Dynamic Biomedical Imaging. Mathematics and Physics of Emerging Biomedical Imaging. Washington (DC): National Academies Press (US); 1996. Chapter 6, Positron Emission Tomography https://www.ncbi.nlm.nih.gov/books/NBK232475/

8. Patton J.A. (2002). Physics of PET. In: Delbeke D, Martin, W.H, Patton J.A, Sandler M.P. (eds) Practical FDG Imaging: A Teaching File. Springer, New York, NY. https://doi.org/10.1007/978-0-387-22453-4_2

9. Ashraf MA, Goyal A. Fludeoxyglucose (18F) [Updated 2023 Aug 28]. In: StatPearls [Internet]. Treasure Island (FL): StatPearls Publishing; 2024 Jan-. Available from: https://www.ncbi.nlm.nih.gov/books/NBK557653/

10. Alberto Del Guerra, Nicola Belcari, Maria Giuseppina Bisogni, Francesco Corsi, Maurizio Foresta, Pedro Guerra, Sara Marcatili, Andres Santos, Giancarlo Sportelli, Silicon Photomultipliers (SiPM) as novel photodetectors for PET, Nuclear Instruments and Methods in Physics Research Section A: Accelerators, Spectrometers, Detectors and Associated Equipment, Volume 648, Supplement 1, 2011, Pages S232-S235, https://doi.org/10.1016/j.nima.2010.11.128

11. Jiang, & Chalich, & Deen,. (2019). Sensors for Positron Emission Tomography Applications. Sensors. 19. 5019. https://doi.org/10.3390/s19225019

12. Al-Haddad R, Ismailani U.H, Rotstein B.H, Current and Future Cardiovascular PET Radiopharmaceuticals, PET Clinics, Volume 14, Issue 2, 2019, Pages 293-305, ISSN 1556-8598, ISBN 9780323678414, https://doi.org/10.1016/j.cpet.2018.12.010

13. Philipp Grätzel von Grätz, The wisdom of water, Siemens Healthineers, Imaging Life, 2023-09-01. https://www.siemens-healthineers.com/fi/molecular-imaging/news/the-wisdom-of-water

14. Sciagrà, R., Lubberink, M., Hyafil, F. et al. EANM procedural guidelines for PET/CT quantitative myocardial perfusion imaging. Eur J Nucl Med Mol Imaging 48, 1040–1069 (2021). https://doi.org/10.1007/s00259-020-05046-9

15. Koivula T, Uurasmaa TM, Han C, Maaniitty T, Latifi S, Lempiäinen S, Kalliokoski K, Sundberg CJ, Rundqvist H, Anttila K, Minn H, Knuuti J, Heinonen I. Myocardial blood flow in newly diagnosed breast cancer patients at rest and during exercise, iScience, Volume 27, Issue 11, 2024, 111081, ISSN 2589-0042, https://doi.org/10.1016/j.isci.2024.111081

16. Yoshinaga K, Klein R, Tamaki N. Generator-produced rubidium-82 positron emission tomography myocardial perfusion imaging—From basic aspects to clinical applications, Journal of Cardiology, Volume 55, Issue 2, 2010, 163-173. https://www.journal-of-cardiology.com/article/S0914-5087(10)00010-9/fulltext

17. Krakauer M, Ismail A, Talleruphuus U, Henriksen AC, Lonsdale MN, Rasmussen IL, Fuglsang S, Prescott E, Hovind P, Marner L. ^{82}Rb and [^{15}O]H_2O myocardial perfusion PET imaging: a prospective head to head comparison. J Nucl Cardiol. 2023 Dec;30(6):2790-2802. https://doi.org/10.1007/s12350-023-03372-7

18. Knuuti J, Tuisku J, Kärpijoki H, Iida H, Maaniitty T, Latva-Rasku A, Oikonen V, Nesterov SV, Teuho J, Jaakkola MK, Klén R, Louhi H, Saunavaara V, Nuutila P, Saraste A, Rinne J, Nummenmaa L. Quantitative Perfusion Imaging with Total-Body PET. J Nucl Med. 2023 Nov;64(Suppl 2):11S-19S. https://doi.org/10.2967/jnumed.122.264870

19. Britannica, The Editors of Encyclopaedia. "cyclotron". Encyclopedia Britannica, 22 Mar. 2024, https://www.britannica.com/technology/cyclotron

20. J. Powell, J.P. O'Neil, Production of [15O] Water at Low-Energy Proton Cyclotrons, Ernest Orlando Lawrence Berkeley National Laboratory, Berkeley, CA 94720, USA. https://www.osti.gov/servlets/purl/891212

21. Hidex RadioWater generator Manual, Ver. 3 8.5.2024 Heidi Partanen, Turku PET Centre internal documentation

22. Henry Hsiao, Radiowater Generator system schematic, 2024. Manufacturers internal schematic, Hidex Oy. Modified in 13.12.2024

23. L. Ziyu, L. Shichao, Y. Zhongmin Structured Scintillators for Efficient Radiation Detection 10.10.2021, Advanced Science – Influence Series. https://doi.org/10.1002/advs.202102439

24. Henry Hsiao, Assembly drawing of the fibre optic scintillator clip, 2024. Manufacturers internal schematic, Hidex Oy. Modified in 13.12.2024

25. Henry Hsiao, PLC system layout in operation schematic, 2024 Manufacturers internal schematic, Hidex Oy. Modified in 3.1.2025

26. M. Bourne, Simpson's Rule – Interactive mathematics, section 6. https://www.intmath.com/integration/6-simpsons-rule.php Cited in 18.12.2024

10 Appendices

Appendix 1. Full width at Half Maximum calculator script

```
import numpy as np
import matplotlib.pyplot as plt
from scipy.signal import find_peaks
from scipy.interpolate import interp1d
from scipy.integrate import simpson  # Updated import

def calculate_fwhm(data):
    max_val = np.max(data)
    half_max = max_val / 2.0

    # Find peaks to determine the peak position
    peaks, _ = find_peaks(data)
    peak_idx = peaks[np.argmax(data[peaks])]

    # Interpolation to find the exact positions at half max
    interp = interp1d(np.arange(len(data)), data - half_max, kind='linear')
    roots = np.where(np.diff(np.sign(interp(np.arange(len(data))))))[0]

    # Ensure we only get the roots around the peak
    left_idx = roots[roots < peak_idx][-1]
    right_idx = roots[roots > peak_idx][0]

    fwhm = right_idx - left_idx

    return fwhm, left_idx, right_idx

def main():
    # Input the dataset
    print("Please enter your dataset, with each value on a new line.")
    print("Press Enter twice when you are done.")

    # Read input until the user submits an empty line
    dataset_str = []
    while True:
        line = input()
        if line == "":
            break
        dataset_str.append(line.strip())

    # Convert input strings to a list of integers
    data = np.array([int(x) for x in dataset_str if x.isdigit()])

    if len(data) == 0:
        print("No valid data was entered. Please ensure your data is numerical.")
        return

    # Calculate FWHM
    fwhm, left_idx, right_idx = calculate_fwhm(data)

    # Calculate AUC for the range 240 to 490
    if len(data) >= 490:
        auc = simpson(data[239:490])  # Python indices are 0-based, so 239 corresponds to the 240th element
    else:
        print("The dataset is too short for the specified AUC range.")
        return

    # Plot data with FWHM marked
    plt.figure(figsize=(12, 6))
    plt.plot(data, label='Data')
    plt.axvline(left_idx, color='r', linestyle='--', label='FWHM Left')
    plt.axvline(right_idx, color='g', linestyle='--', label='FWHM Right')
    plt.axhline(np.max(data) / 2, color='b', linestyle='--', label='Half Maximum')
    plt.axvspan(239, 489, color='gray', alpha=0.2, label='AUC Range (240th to 490th)')
    plt.legend()
    plt.title(f'Data with FWHM and AUC\nFWHM: {fwhm}, AUC (240th-490th): {auc}')
    plt.xlabel('Index')
    plt.ylabel('Value')
    plt.show()

    # Display the results
    print(f"Full Width Half Maximum (FWHM): {fwhm}")
    print(f"Area Under the Curve (AUC) from 240th to 490th value: {auc}")

if __name__ == "__main__":
    main()
```